Tectonophysics 811 (2021) 228887

Contents lists available at ScienceDirect

Tectonophysics

journal homepage: www.elsevier.com/locate/tecto

Impact of salt layers interaction on the salt flow kinematics and diapirism in the Eastern Persian Gulf, Iran: Constraints from seismic interpretation, sequential restoration, and physical modelling

Jafar Hassanpour [a], Josep Anton Muñoz [b,*], Ali Yassaghi [a], Oriol Ferrer [b], Salman Jahani [c], Pablo Santolaria [b], Seyed Mohsen SeyedAli [d]

[a] *Department of Geology, Tarbiat Modares University, Tehran, Iran*
[b] *Institut de Recerca Geomodels, Departament de Dinàmica de la Terra i de l'Oceà, Facultat de Ciències de la Terra, Universitat de Barcelona, Barcelona, Spain*
[c] *National Iranian Oil Company, Exploration Directorate, Tehran, Iran*
[d] *Iranian Offshore Oil Company, Tehran, Iran*

A R T I C L E I N F O

Keywords:
Persian Gulf
Salt tectonics
Differential sedimentary loading
Diapir squeezing
Salt sheet
Physical modelling
Sequential restoration

A B S T R A C T

Interpretation of reflection seismic profiles, sequential restoration, and physical modelling are presented to understand the kinematics of salt flow and diapirism in the Eastern Persian Gulf, offshore Southern Iran. Salt tectonics in this area result from the overlapping Ediacaran–Early Cambrian Hormuz Salt, which is regionally present, and Oligocene–Early Miocene Fars Salt, which is locally developed. The Hormuz and Fars salts began flowing at Cambrian(?) and Early Miocene times, respectively. Diapirs fed by the Hormuz Salt rose passively during Palaeozoic and Mesozoic times and were rejuvenated by contractional deformation events in the Cenozoic. Fars-Salt structures exist either as salt walls and anticlines around those diapirs of Hormuz Salt that developed allochthonous salt bodies during a Palaeocene–Eocene contractional squeezing before deposition of the Fars Salt, or as gentle shallow salt pillows above deep pillows of Hormuz Salt, suggesting a kinematic linkage. Flow of Fars Salt was mainly triggered by differential sedimentary loading. It seems that its lateral flow kinematics was controlled by the behaviour of the underlying Hormuz-Salt sheets. More than ~10-km-long salt sheets were efficiently evacuated back towards the Hormuz-Salt diapir, and consequently, maintained the Fars-Salt evacuation and flow to the same direction, accompanied by welding of both salt layers. Conversely, smaller, less than ~3-km-long salt sheets allowed limited salt evacuation or rearrangement that was probably still sufficient to trigger Fars-Salt flow near the central (Hormuz-Salt) diapir. Fars-Salt evacuation was enhanced by differential sedimentary loading, resulting in incipient primary welds. Subsequently, the depocentres migrated towards the areas of available Fars Salt away from the central diapir. In both cases, layer-parallel shortening related to regional contraction probably played also a role in triggering the Fars-Salt flow at Early Miocene, but was more influential at later stages by squeezing the salt structures (Hormuz and Fars) since about Late Miocene onwards.

1. Introduction

Salt is a viscous, low-strength and incompressible rock (e.g. Weijermars et al., 1993). Over geological timescales, this makes salt prone to flow (Weijermars et al., 1993; Rowan et al., 2004; Hudec and Jackson, 2007) if the forces driving salt deformation overcome the forces resisting salt deformation (Jackson and Hudec, 2017). Consequently, the mobile salt may result in evacuation and inflation of salt and the formation of diapiric structures such as salt walls and stocks, or allochthonous salt sheets. Salt can also remain buried as salt pillows and anticlines. Initiation of these salt structures may be driven in several ways. The most important mechanisms consist of differential sedimentary loading (Ge et al., 1997; Gemmer et al., 2004; Vendeville, 2005; Hudec and Jackson, 2007; Warsitzka et al., 2013; Rowan, 2019), regional extension (Vendeville and Jackson, 1992; Jackson and Vendeville, 1994), gravity-driven spreading and gliding (Letouzey et al., 1995; Rowan et al., 2004; Brun and Fort, 2011), and contractional deformation including rejuvenation of preexisting salt structures (e.g. Letouzey et al., 1995; Del

* Corresponding author.
E-mail address: jamunoz@ub.edu (J.A. Muñoz).

https://doi.org/10.1016/j.tecto.2021.228887
Received 8 December 2020; Received in revised form 16 April 2021; Accepted 19 April 2021
Available online 23 April 2021

Ventisette et al., 2005; Duffy et al., 2018; Santolaria et al., 2021) as well as amplification and breaching of contractional salt-cored detachment folds (Stewart and Coward, 1995; Bonini, 2003; Rowan and Giles, 2021).

Salt structures initiated by any of these mechanisms may evolve to passive diapirs (Rowan et al., 2003; Hudec and Jackson, 2007), in which the diapir crest is at or just beneath the seafloor or ground surface (Rowan and Giles, 2021). The inflated salt body generally passes through a relatively rapid active diapirism stage during which the pressurised salt pierces through its roof weakened by erosion or extension (Schultz-Ela et al., 1993) to allow the diapir become a passive diapir. Passive diapirs commonly grow by differential loading imposed from overburden (gravitational loading) (e.g. Hudec and Jackson, 2007) but may also be rejuvenated by lateral contraction (Vendeville and Nilsen, 1995; Dooley et al., 2009a; Duffy et al., 2018; Hassanpour et al., 2020).

Most of the world's salt-bearing sedimentary basins contain considerable hydrocarbon accumulations (see e.g. Warren, 2016). It is, therefore, critical to understand the tectonosedimentary record of salt movement and diapirism in these basins. This may include exploring the spatial distribution of the salt layers and salt structures, investigating their temporal evolution, and deciphering their impact on the sediment dispersal and facies distribution within the basin (Warren, 2016; Jackson and Hudec, 2017). The structural evolution of the salt structures is commonly deciphered by studying the outcropping country rocks (e.g. Giles and Lawton, 2002; Jahani et al., 2007; Snidero et al., 2019) or by the interpretation of reflection seismic data (e.g. Trusheim, 1960; Davison et al., 2000; Jackson and Hudec, 2017), but may also be explored by carrying out sequential restoration (e.g. Rowan, 1993; Rowan and Ratliff, 2012; Hassanpour et al., 2020), as well as physical (Vendeville and Jackson, 1992; Dooley et al., 2009a; Warsitzka et al., 2015; Duffy et al., 2018) and numerical modelling (Schultz-Ela, 2003; Albertz et al., 2010; Pichel et al., 2017).

In the Southeastern Zagros and the Persian Gulf (Southern Iran), a large number of emergent and buried salt structures (Fig. 1a) have been formed by diapirism of the Ediacaran–Early Cambrian Hormuz Salt (Fig. 2), deposited after ca. 558 ± 7 Ma (Faramarzi et al., 2015). The Hormuz Salt has also been reported southwards in the United Arab Emirates and Saudi Arabia (Kent, 1979; Edgell, 1996; Stewart, 2016, 2017), as well as in Oman (Ara Salt, e.g. Droste, 1997) deposited between 547 Ma and 536 Ma (Fig. 2) (Allen, 2007; Bowring et al., 2007; Al-Husseini, 2014, 2015). In the Eastern Persian Gulf, a younger local salt horizon known as Fars Salt (Fig. 1a) (Jahani et al., 2009) of Oligocene–Early Miocene age (Fig. 2) has also formed few salt structures (Fig. 1b). The overlap and interaction of these mobile salt layers have led to a distinctive salt-related structural style in the Eastern Persian Gulf relative to the surrounding areas.

Interpretation of seismic data from the Persian Gulf suggests that the Hormuz Salt began flowing at the Early Palaeozoic (Jahani et al., 2009, 2017; Perotti et al., 2016) probably during deposition of the Cambrian strata directly above the salt (Hassanpour et al., 2020; Snidero et al., 2020). This is in agreement with thinning of the drilled Cambrian deposits above Hormuz-Salt pillows in the Northeast Saudi Arabia south of the Persian Gulf (Stewart, 2017). This also matches the evidence of Ara-Salt movement during deposition of the Lower Cambrian Nimr Group (Fig. 2) directly above the salt layer (e.g. Li et al., 2012). Differential sedimentary loading has been suggested as the principal driving force for the subsequent long-term development of Hormuz-Salt structures. Later on, they were rejuvenated by the Palaeocene–Eocene contractional deformation of the Oman Mountains (Hassanpour et al., 2020; Snidero et al., 2020) and the Late Cenozoic Zagros compression (Letouzey and Sherkati, 2004; Jahani et al., 2009, 2017; Callot et al., 2012; Hassanpour et al., 2018; Snidero et al., 2019).

In contrast to the Hormuz Salt, the Fars Salt stratigraphy is constrained by wells drilling the Fars Salt interval (Fig. 1b), showing a massive pure halite at the lower and middle parts overlain by interbedded halite, anhydrite and claystone in the upper part (Orang et al., 2018). Based on seismic profiles interpretation, the Fars Salt flowed

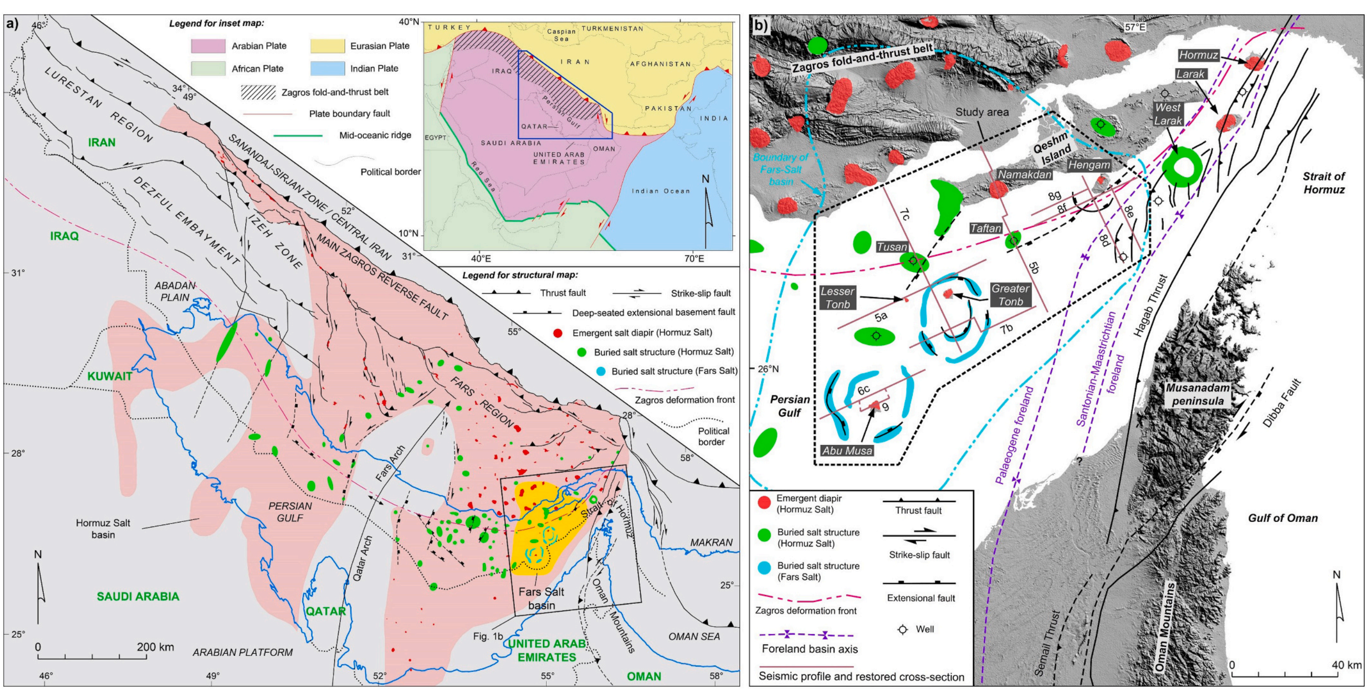

Fig. 1. a) Regional structural map illustrating major structural elements of the Zagros fold-and-thrust belt, Persian Gulf, Strait of Hormuz, and the Northern Oman Mountains, along with the extents of the Hormuz and Fars salts basins (pink and yellow, respectively) and distribution of their salt structures (modified after Berberian, 1995; Searle, 2007; Jahani et al., 2009, 2017; Stewart, 2017; Hassanpour et al., 2020). Inset shows the location of the region along the northeast margin of the Arabian Plate. b) Structural map of the Eastern Persian Gulf and adjacent areas showing the major faults and distribution of emergent and buried salt structures (Hassanpour et al., 2020). The Oman faults are based on Ali and Watts (2009) and Searle et al. (2014). The study area is outlined by a dashed black polygon. (For interpretation of the references to colour in this figure legend, the reader is referred to the web version of this article.)

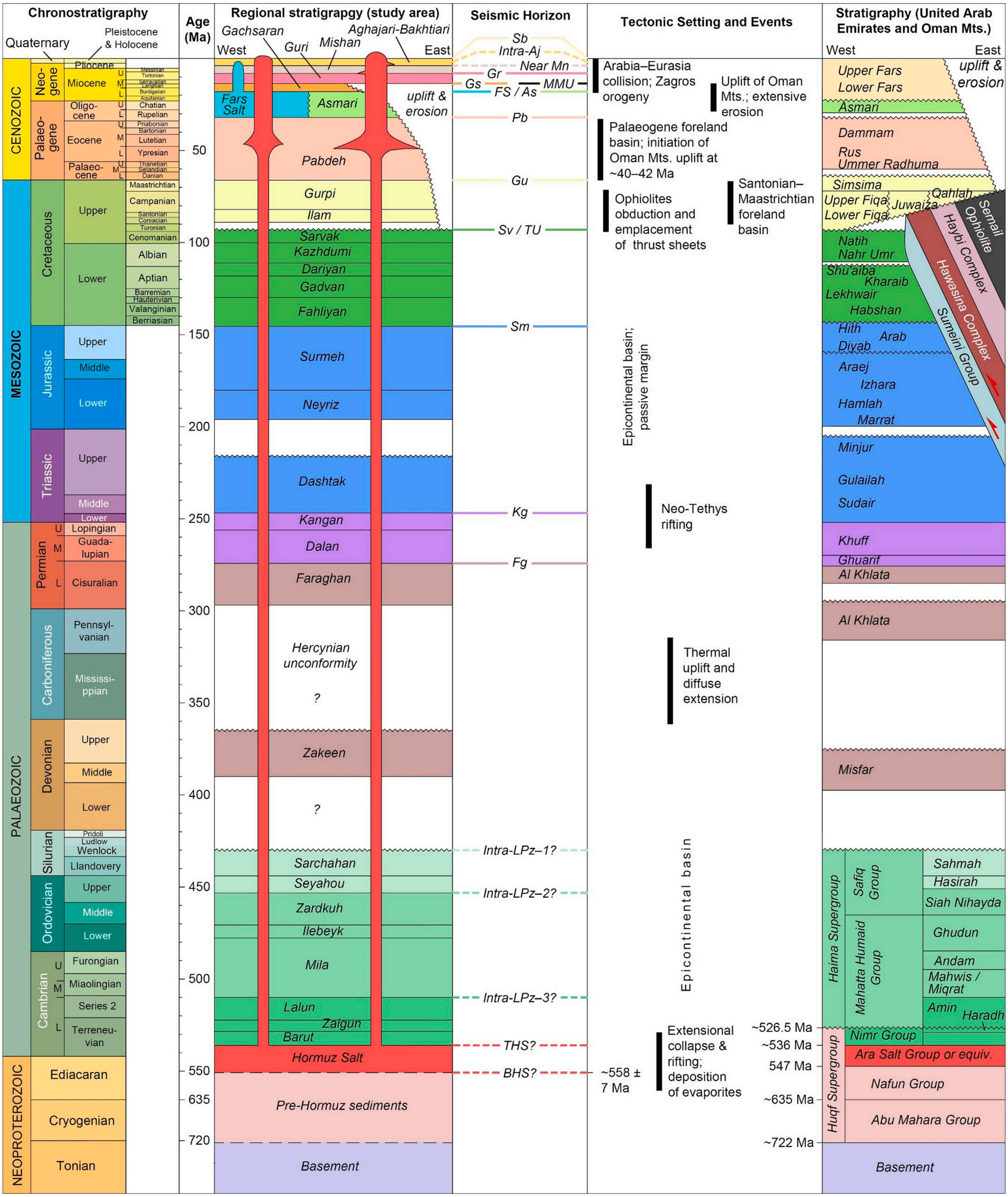

Fig. 2. Simplified stratigraphic chart and major tectonic events of the Eastern Persian Gulf (left) along with the equivalent chart of the eastern part of the United Arab Emirates and the Oman Mountains (right). The chart is taken from Hassanpour et al. (2020) based on compilation and modifications of previously published information (James and Wynd, 1965; Allen, 2007; Bowring et al., 2007; Ali and Watts, 2009; Jahani et al., 2009; Piryaei et al., 2011; Al-Husseini, 2014, 2015). Approximate age of the base of Hormuz Salt is based on Faramarzi et al. (2015) and age of pre-Hormuz sediments is considered equivalent to the Oman chart. Note that the geological timescale older than 550 Ma is nonlinear. Abbreviations of the seismic reflectors: BHS: base Hormuz Salt; THS: top Hormuz Salt; Intra-LPz–3 to Intra-LPz–1: seismic reflectors inside the Lower Palaeozoic succession; Fg: top Faraghan Fm.; Kg: top Kangan Fm.; Sm: top Surmeh Fm.; Sv: top Sarvak Fm.; Gu: top Gurpi Fm.; Pb: top Pabdeh Fm; FS: top Fars Salt; Gs: top Gachsaran Fm.; Gr: top Guri; Near Mn: Near top Mishan Fm.; Intra-Aj: Intra-Aghajari Fm.; Sb: Seabed.

since the Early Miocene (Jahani et al., 2009; Orang et al., 2018; Ezati Asl et al., 2019; Faghih et al., 2019; Hassanpour et al., 2020; Snidero et al., 2020). As a result, minibasins and primary salt welds were developed due to the salt evacuation (Hassanpour et al., 2020; Snidero et al., 2020). Salt flow led to the formation of some ring-like salt walls and salt anticlines peripheral to few major preexisting diapirs of the Hormuz Salt (Fig. 1b); in addition, few Fars-Salt pillows were developed above preexisting deep-seated Hormuz-Salt pillows.

In spite of several studies on the Fars Salt, the kinematics of its flow is still debated. Open questions on its temporal and spatial movement are: Why has it flowed only around some of the Hormuz-Salt diapirs? What factors controlled the dominant flow direction of the Fars Salt around these Hormuz-Salt diapirs? To address these questions and to better constrain the kinematics of Fars-Salt flow and diapirism, here, we present interpreted 2D seismic profiles and sequentially restore one of them to decipher the evolving geometries of the salt structures. We then compare the results with two physical models testing the interaction of the Hormuz and Fars salts and the controlling factors on the kinematics of the salt flow.

2. Geological setting

The Persian Gulf is part of a hydrocarbon-rich foreland basin bounded to the northeast by the NW–SE trending Zagros Mountains and to the east by the N–S trending Oman Mountains (Fig. 1). The Zagros and Oman orogenic belts resulted from the Arabia–Eurasia convergence and continental collision closing the Neo-Tethys Ocean that separated the present-day Zagros from Central Iran (Glennie et al., 1974; Berberian and King, 1981; Agard et al., 2011; Frizon de Lamotte et al., 2011; Mouthereau et al., 2012). The study area is located at the eastern part of the Persian Gulf that is bounded to the north by the Southeastern Zagros fold-and-thrust belt, to the southeast by the Northern Oman Mountains, and to the southwest by the Arabian Platform (Fig. 1a,b).

The basement of the present-day Arabian Plate resulted from the Neoproterozoic oceanic crust subduction and amalgamation of continental fragments and volcanic arcs along the northeast margin (present-day coordinates) of the African Plate (e.g. Nehlig et al., 2002; Stern and Johnson, 2010). Subsequently, extensional collapse of the Arabian–Nubian Shield at ca. 620–530 Ma provided favourable conditions for deposition of the Hormuz Salt, mainly in Southern Iran and Northeastern Saudi Arabia (Fig. 1a), and equivalent evaporites in adjacent regions, such as the Ara Salt in Oman and the Salt Range Formation in Pakistan (e.g. Edgell, 1996; Al-Husseini, 2000).

Deposition of the Hormuz Salt was followed during the Early Palaeozoic by a relatively stable platform dominated by clastic sedimentation until Middle Devonian times (e.g. Berberian and King, 1981; Faqira et al., 2009). A major pre-Permian unconformity (Hercynian unconformity) has been recognised in the High Zagros (Tavakoli-Shirazi et al., 2013) and Arabia (Faqira et al., 2009; Stewart, 2016, 2017). It is suggested to result from regional-scale vertical movements likely driven by thermal uplift of the lithosphere between the Late Devonian and the Early Carboniferous (Tavakoli-Shirazi et al., 2013). In the Late Permian–Early Triassic, rifting and continental breakup led to the initiation of the Neo-Tethys Ocean separating Africa–Arabia in the south from Eurasia in the north (Stöcklin, 1968; Alavi, 2004). Intra-oceanic subduction of the Neo-Tethys was followed by the obduction of the oceanic crust together with deepwater and slope sediments onto the northeastern margin of Arabia since Cenomanian–Turonian times (Glennie et al., 1974; Berberian and King, 1981). Obduction led to the emplacement of the Semail (Oman) and Zagros ophiolites stacked with few other thrust sheets (Fig. 2) (Boote et al., 1990; Ali and Watts, 2009; Frizon de Lamotte et al., 2011; Searle et al., 2014). Thrust activity related to this process ended at ca. 70 Ma (Early Maastrichtian) (Searle, 2007).

The Neo-Tethys Ocean was closed by the onset of the Arabia–Eurasia collision at ca. 27 Ma (Pirouz et al., 2017) or possibly earlier at ca. 35–30 Ma (Agard et al., 2011; Frizon de Lamotte et al., 2011; Mouthereau et al., 2012). The collision and crustal thickening was succeeded by the initiation of the present-day Zagros and Oman orogenic belts since Late Oligocene, which climaxed at Early Miocene in Oman (Boote et al., 1990; Searle et al., 2014) although uplift of the Oman Mountains initiated earlier (Late Eocene) at ca. 40–42 Ma (Hansman et al., 2017; Corradetti et al., 2020). In the Southeastern Zagros, the main phase of folding was progressive from the northeast to the southwest: folding initiated at ca. 26–21 Ma in the northeast close to the Neo-Tethys Ocean suture zone (Pirouz et al., 2015, 2017) and advanced southwestward. Therefore, the central part of the Fars region in the Southeastern Zagros was folded between ca. 14–15 Ma at the northeast (Khadivi et al., 2012) and ca. 4.65 (Najafi et al., 2020) to ca. 3.8 Ma (Ruh et al., 2014) at the southwest. Folding eventually progressed further towards the southwest into the Persian Gulf (Hessami et al., 2001).

3. Methods

3.1. Seismic data and interpretation

Our data consist of post-stack and time-migrated 2D reflection seismic profiles, which have been chosen from a regular 2 × 2 km network covering the Iranian sector of the Persian Gulf (Fig. 1b). These seismic profiles reach a recording depth of 6–7 s two-way time (TWT), and are oriented in two directions perpendicular to each other. The 2D seismic network does not cover the diapirs exposed in the islands and the shallow waters around them as seismic acquisition was marine. However, the Qeshm Island, which contains few anticlines and one exposed salt diapir, is traversed by few sparse land-acquisition 2D seismic profiles. They have comparatively lower quality especially at the deeper part.

Drilled formation tops were tied to the seismic profiles using available velocity data. The wells across our studied area drilled to a maximum depth of ~4700 m below the mean sea level reaching the Lower Cretaceous Fahliyan Formation (Fig. 2). We interpreted a total of 18 main seismic reflectors or events from the present-day seafloor down to the base of the Hormuz Salt (see Fig. 2), as well as five additional reflectors within the Guri and Gachsaran intervals along some profiles. The upper seismic reflectors from Seabed (Sb) down to the Upper Cretaceous Sarvak Formation (Sv) / Turonian Unconformity (TU) were tied to the wells across the study area. The deeper ones in the Jurassic, Triassic and Permian sediments (Sm, Kg and Fg reflectors; Fig. 2) have been traced from other seismic profiles of the regular seismic network westward over the Central Persian Gulf where the wells penetrated the Permian strata. The underlying three seismic reflectors within the Lower Palaeozoic (Intra-LPz–1, 2 and 3 reflectors) have unknown ages. The reflectors corresponding to the top and base of the Hormuz Salt are the deepest ones and are traced from few locations in the Eastern Central Persian Gulf, where the salt is imaged in deep pillows bounded by primary welds (see Jahani et al., 2017, their Fig. 9).

The time-interpreted seismic reflectors were converted into depth domain using interval velocities that were extracted from checkshots and sonic logs from the wells in the study area and some others in Central Persian Gulf. For the intra-Lower Palaeozoic sediments that have not been drilled by the wells, Jahani et al. (2009) assumed an average velocity of 4500 m/s. However, we assumed an average interval velocity of 5000 m/s for these deposits considering their dominantly siliciclastic lithology at a burial depth of more than ~7–8 km. This velocity is more compatible with the velocity calculated from the empirically-derived P-wave and bulk density relationship of siliciclastic rocks (Gardner et al., 1974; Miller and Stewart, 1991) according to their compaction at these burial depths. The Hormuz Salt was converted using an interval velocity of 4500 m/s that is appropriate for salt-bearing formations composed predominantly of halite interlayered with other sedimentary rocks (evaporites and nonevaporites) as well as some encased volcanic blocks (e.g. Jackson and Hudec, 2017). Based on well data, a similar average interval velocity of ~4400 m/s has been reported for the Aptian salt in the Santos Basin, offshore Brazil (Rodriguez et al., 2018).

3.2. Sequential cross-section restoration

The depth-converted seismic interpretations were subsequently used for the sequential cross-section restoration. Step-by-step, standard cross-section restoration (e.g. Rowan, 1993; Rowan and Jarvie, 2020) was carried out by removing fault displacements (if present), unfolding the sedimentary sequence, and decompaction accompanied by isostatic adjustment. Fault displacements were restored by fault-parallel flow or elliptical fault flow methods. Sequential unfolding of the section was performed using vertical simple shear or flexural-slip unfolding algorithms depending on whether the deformation occurred by vertical or lateral movements, respectively. The Sclater-Christie compaction function (Sclater and Christie, 1980), which appropriately models sedimentary compaction in areas of mixed lithologies, was employed for decompacting the sediments in response to stripping off top layers during each stage. This compaction function, known also as Athy's relation (Athy, 1930), is written as:

$$\varphi = \varphi_0 e^{-cz} \quad (1)$$

where φ is the porosity (fraction) at depth z (km), φ_0 is the initial porosity (fraction) at surface, and c is the compaction coefficient (km^{-1}), which depends on the lithology and determines the rate of porosity decay with increasing depth.

To use this function, we calculated mean decompaction parameters (φ_0 and c) for each interval considering the percentages of the contained dominant lithologies and corresponding standard decompaction parameters (Table 1). Standard values for φ_0 and c have been derived from the literature (e.g. Sclater and Christie, 1980; Schmoker and Halley, 1982; Berra and Carminati, 2010) (Table 1).

3.3. Physical modelling

3.3.1. Rationale, model setup, and procedure

No physical or numerical modelling has studied diapirism and salt interaction in a multiple salt layer system so far, because such a prototype is relatively less common. Inspired by the characteristic structural style resulting from the interaction between Hormuz-Salt structures and

Table 1
Decompaction parameters used for decompaction of intervals during restoration of the cross-section. For the Fars Salt and Hormuz Salt intervals (*), percentages are derived from well data (Fars Salt) or estimated according to the known general stratigraphy (Hormuz Salt). However, the nonevaporite values of these two intervals were set to zero to model them with pure salt (halite) decompaction parameters.

Rock type or lithology	Conglomerate	Sandstone	Siltstone	Shale	Marl	Limestone	Dolomite	Anhydrite	Halite
Initial porosity, φ_0 (fraction)	0.30	0.49	0.56	0.63	0.57	0.51	0.30	0	0
Compaction coefficient, c (km^{-1})	0.30	0.27	0.39	0.51	0.51	0.52	0.22	0	0
Mean density of grains, ρ ($kg{\cdot}m^{-3}$)	2690	2650	2680	2720	2675	2710	2870	2960	2160

Horizon	Interval	Lithology percentage (%)									Final decompaction parameters		
		Conglomerate	Sandstone	Siltstone	Shale	Marl	Limestone	Dolomite	Anhydrite	Salt	Total φ_0 (fraction)	Total c (km^{-1})	Total ρ ($kg{\cdot}m^{-3}$)
Sb	Bakhtiari and Upper Aghajari	10	25	0	65	0	0	0	0	0	0.56	0.43	2700
Intra-Aj	Lower Aghajari	0	10	5	45	25	15	0	0	0	0.58	0.48	2698
Near Mn	Mishan	0	0	0	25	50	25	0	0	0	0.57	0.51	2695
Gr	Guri	0	0	0	15	80	5	0	0	0	0.58	0.51	2684
Gs	Gachsaran	0	0	0	0	50	15	0	35	0	0.36	0.33	2780
As	Asmari	0	15	0	5	0	65	15	0	0	0.48	0.44	2726
FS	Fars Salt*	0	0	0	10	10	0	0	10	70	0.12	0.10	2348
Pb	Pabdeh	0	0	0	35	55	10	0	0	0	0.59	0.51	2694
Gu	Gurpi / Tarbur and Ilam	0	10	5	20	55	10	0	0	0	0.57	0.48	2685
Sv / TU	Sarvak, Kazhdumi, Dariyan, Gadvan and Fahliyan	0	0	0	10	25	60	5	0	0	0.53	0.50	2710
Sm	Surmeh, Neyriz and Dashtak	0	0	0	10	10	15	50	15	0	0.35	0.29	2825
Kg	Kanagn and Dalan	0	0	0	5	5	20	55	15	0	0.33	0.27	2834
Fg	Faraghan and Zakeen	0	65	5	30	0	0	0	0	0	0.54	0.35	2673
Intra-LPz–1	?Sarchahan and Seyahou	0	35	0	40	10	15	0	0	0	0.56	0.43	2690
Intra-LPz–2	?Zardkuh, Ilbeyk and Mila	0	20	5	40	5	15	15	0	0	0.53	0.41	2723
Intra-LPz–3	?Lalun, Zaigun and Barut	0	40	10	30	0	10	10	0	0	0.52	0.37	2702
THS	Hormuz Salt*	0	5	0	5	5	5	5	5	70	0.13	0.10	2341
BHS	Pre-Hormuz sediments	0	25	25	30	0	10	10	0	0	0.53	0.39	2707

the Fars Salt, we designed a set of two physical models aiming to understand the influence of shortened, preexisting salt bodies in the halokinesis and resulting geometries of a younger salt horizon. The autochthonous Hormuz and Fars salt layers are separated by a mechanically strong thick (~9–12 km) sedimentary interval (Hassanpour et al., 2020). These models were carried out in an 85-cm-long, 70-cm-wide, and 35-cm-deep glass-sided deformation rig closed by two metal end walls orthogonal to the glass side walls. One of the metal end wall remained fixed during the experiment, whereas the other was attached to a motor-driven worm screw during the contractional deformation playing the role of a contractional backstop (hinterland) (Fig. 3a,b). Our models embrace two situations: the polymer analogous to the Fars Salt either covers a sand sequence having a Hormuz-Salt-equivalent pillow at the base (Fig. 3c) or directly overlies a Hormuz-Salt-equivalent stock (Fig. 3d), showing that the Hormuz-Salt diapirs were at or just beneath the surface during deposition of the Fars Salt. The physical models were shortened up to 7.2 cm (Model 1) and 5.7 cm (Model 2) at a constant velocity of 3 mm/h.

The two physical models include a Hormuz-Salt-equivalent, 1.5-mm-thick, blue polymer layer representing an almost welded salt horizon at the base of the model ignoring the presence of pre-Hormuz sediments above the basement. On top of it, a salt pillow and a salt stock with a pedestal, shaped by bowls, were created using the same polymer. The diapiric stem of the stock was built by shaping blue polymer using plastic moulds made with a 3D printer that allows constraining the geometry of the salt body (Dooley et al., 2015; Santolaria et al., 2021). Even though this methodology is a simplification that does not consider the diapir's triggering mechanism or passive growth of it (Dooley et al., 2009a), it allows simulating the downbuilding geometries at the same time that ensures the reproducibility of salt structures in different models. In both models, the construction of the salt stock was achieved by adding blue polymer layers with a constrained shape until reaching a 6.5-cm-tall salt body (Fig. 3d). Simultaneously to each polymer layer, alternating layers of white and coloured sand were poured and levelled with a mechanical scraper (Krantz, 1991; Lohrmann et al., 2003) in order to keep the geometry of the salt body. Whereas in Model 1 both salt structures were located at 50 cm of the initial position of the moving wall, in Model 2 the salt pillow was shifted by 10 cm towards the hinterland (Fig. 3b). This was performed to test the effect of the salt pillow distance from the backstop (hinterland) on its reactivation during contractional deformation. The setup was similar to that of Santolaria et al. (2021) that considered a contractional brittle-ductile wedge with preexisting salt bodies as the ones we include. They tested several parameters such as the thickness of the source layer and the overburden, the diapir roof thickness, and the location of salt bodies with respect to the backstop. Since we aimed to simulate the rejuvenation of salt structures located far from the deformation front and considering Santolaria et al. (2021) results, we adjusted the location of our salt bodies and the thickness of the salt-sand sequence.

Both salt structures were buried by a 6.5-mm-thick green polymer layer simulating the Fars Salt (Fig. 3a,b). In this case, the polymer did not cover the entire model and has inner and outer pinch-outs located at 35 cm and 75 cm away from the backstop (Fig. 3). This upper polymer and its lateral equivalent white sand layer were covered by a 2-mm-thick pre-contractional blue sand layer (Fig. 3c,d). Whereas Model 1 was shortened after the deposition of this blue sand layer, in Model 2, the pre-contractional sand directly above the upper polymer was vacuumed off following a predetermined annular strip around the deep-rooted salt stock. This was performed to test the reproducibility of annular salt walls of the Fars Salt around the central Abu Musa and Greater Tonb diapirs (Figs. 6 and 7). This caused the upper polymer to start flowing and rise due to differential sedimentary loading, similar to those in Rowan and Vendeville (2006). Sand removal was performed to initiate salt flow by differential sedimentary loading as other processes such as regional extension, progradation, or tilting have not been documented in the Eastern Persian Gulf during the Early Miocene when the Fars Salt was first mobilised (Hassanpour et al., 2020; Snidero et al., 2020). Instead, the sharply truncated oldest overburden layers at the flanks of the annular salt walls (Figs. 6 and 7) suggest that local erosion played an important role to allow the diapiric rise of the inflated Fars Salt. The upper polymer continued to rise under pure gravitational loading and evolved into a salt wall; at the same time, two additional sand layers were deposited. This stage was followed by contractional deformation and deposition of syn-contractional sand layers at regular time intervals of 3.5 h until the end of the experiment. Since the onset of shortening delayed in Model 2, five syn-contractional layers were added instead of six as in Model 1. The regional was raised by 2 mm before the deposition of each syn-contractional sand layer. These sands were also levelled to their regional datum by the mechanical scraper.

At the end of the experiment, both models were covered by a thick postkinematic sand layer to preserve the final topography and inhibit any undesired polymer movement. The models were subsequently serially sectioned into 3-mm-thick vertical slices.

3.3.2. Physical model materials and scaling

To simulate the overburden, we used a frictional dry silica sand (white and coloured, different colours but same rheology) with an average grain size of 200 μm (Ferrer et al., 2017; Roma et al., 2018b; Pla et al., 2019), which deforms according to the Mohr-Coulomb failure criterion at moderate to high values of normal stress (Hubbert, 1951; Horsfield, 1977). The used sand has an internal friction angle of 34.6°, a bulk density of 1500 kg·m^{-3}, a coefficient of internal friction of 0.69, and a low apparent cohesive strength of 55 Pa (Ferrer et al., 2017). In contrast, the polydimethylsiloxane (PDMS) polymer analogous to the natural rock salt has a near-perfect Newtonian viscous fluid behaviour with a density of 974 kg·m^{-3} at room temperature and a viscosity of 1.6 $\times$ 10^4 Pa·s (Dell'Ertole and Schellart, 2013) when deformed at a laboratory strain rate of 10^{-4} s^{-1} (Weijermars et al., 1993). A summary of the scaling parameters is shown in Table 2.

The sandpack overburden thicknesses above the two polymer layers were scaled to the natural analogue (Eastern Persian Gulf) according to a geometric similarity ratio of 6.5 $\times$ 10^{-6}, meaning that 6.5 mm in the model corresponds to 1 km in nature (Table 2). Thickness of the upper polymer (green) was also scaled by the same ratio to the ~1 km depositional thickness of the Fars Salt (Table 2) derived from well and seismic data, as well as cross-section restoration (Hassanpour et al., 2020).

The dynamic viscosity of the Hormuz Salt in the Hormuz and Namakdan diapirs (Fig. 1b for location) in the Eastern Persian Gulf is estimated to be in the range of 10^{18}–10^{21} Pa·s and 10^{17}–10^{21} Pa·s, respectively (Mukherjee et al., 2010). The average viscosity of salt in these diapirs is, therefore, assmued to be ~10^{19} Pa·s. This is also in agreement with the viscosity of diapiric salt having a typical grain size of 10 mm, where a viscosity of 10^{18} Pa·s and 10^{19} Pa·s is representative of salt at the surface and at depth, respectively (Jackson and Hudec, 2017). According to this, in many physical models of salt tectonics, the salt viscosity is assumed to be 10^{18}–10^{19} Pa·s, leading to the scaling of the models to the natural prototype using a viscosity ratio of 10^{-14}–10^{-15} (e.g. Callot et al., 2007; Dooley et al., 2009a, 2015; Ferrer et al., 2017; Roma et al., 2018b; Pla et al., 2019).

We take these considered salt viscosities in the literature and those estimated by Mukherjee et al. (2010) for the Namakdan and Hormuz diapirs to assume an average viscosity of 10^{19} Pa·s for salt, resulting in a viscosity ratio of 1.6 $\times$ 10^{-15} in our models (Table 2). Considering this viscosity ratio along with time (4.5 $\times$ 10^{-10}), length (6.5 $\times$ 10^{-6}) and stress (3.6 $\times$ 10^{-6}) ratios, as well as shortening duration of the models (24 h in Model 1 and 19 h in Model 2), the shortening rate of 3 mm/h in the models approximates ~2 mm/yr shortening rate in nature during ~5–6 myr. This rate is consistent with ~2 mm/yr (Vergés et al., 2018) and ~4 mm/yr (Najafi et al., 2020) of regional shortening in the northwest (Lurestan) and southeast (Fars) regions, respectively, of the Zagros fold belt during the Miocene and Pliocene, and 1–2 mm/yr of Eocene contractional deformation in the Oman Mountains (Hansman

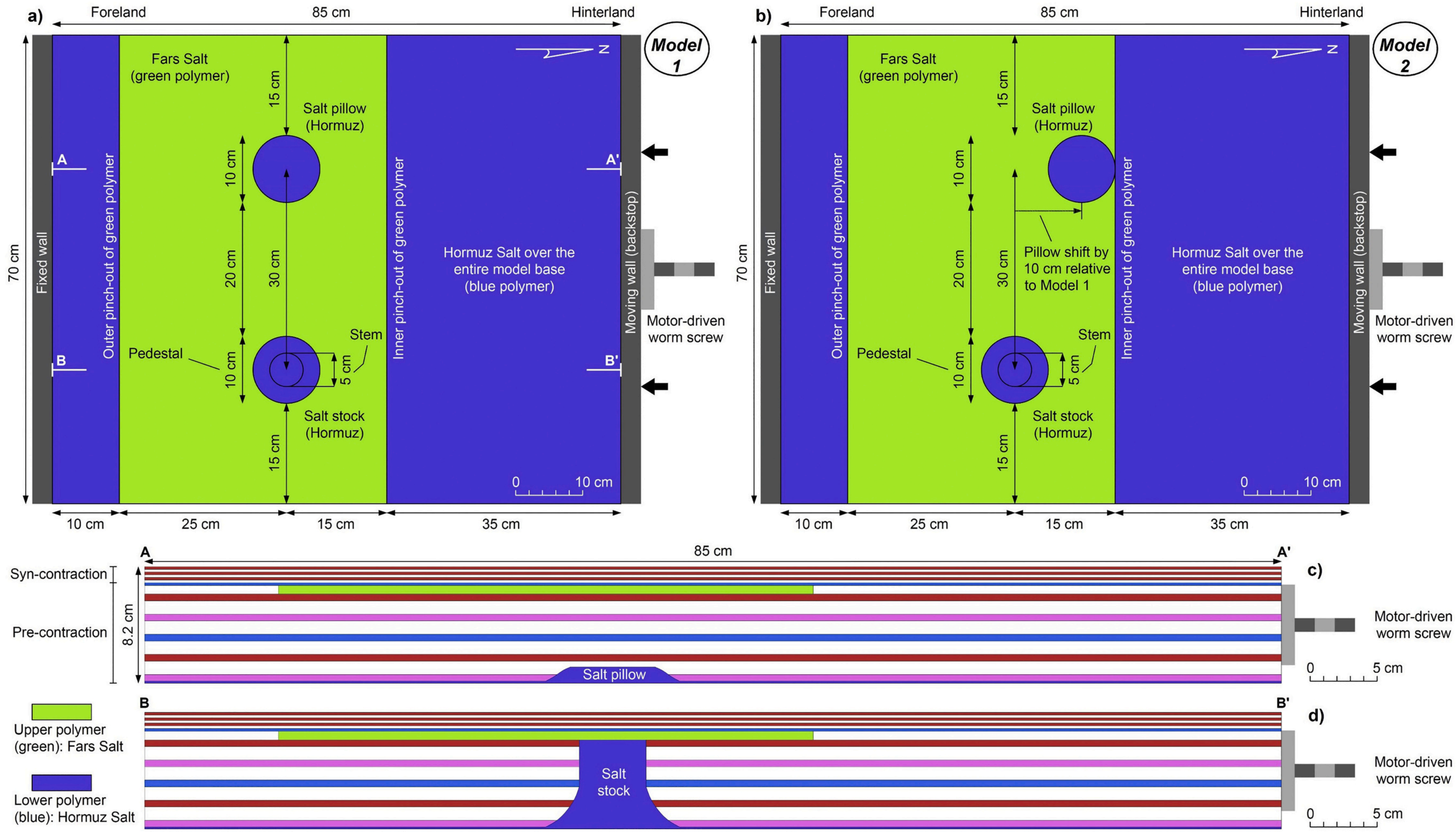

Fig. 3. Setup of the physical models. Plan-view distribution of the polymer layers, blue for the Hormuz Salt equivalent and green for the Fars Salt equivalent, in Model 1 (a) and Model 2 (b). The lower panel illustrates schematic cross-sections through the salt pillow (c) and salt stock (b) of Model 1 depicted at the beginning of the experiments (see location in Fig. 3a). In Model 2, the location of the salt pillow was shifted 10 cm towards the moving wall. (For interpretation of the references to colour in this figure legend, the reader is referred to the web version of this article.)

Table 2
Physical model materials and scaling parameters used in the experimental program. *Viscosities of the rock salt are from estimations provided by Mukherjee et al. (2010) on the Hormuz and Namakdan salt diapirs in the Eastern Persian Gulf.

Parameter	Model	Nature	Model / Nature ratio
Thickness of sand above the upper polymer (Fars Salt)	14 mm	2150 m (average regional thickness)	6.5×10^{-6}
Thickness of the upper polymer (Fars Salt)	6.5 mm	1000 m	6.5×10^{-6}
Thickness of sand between the upper (Fars Salt) and lower (Hormuz Salt) polymers	65 mm	10,000 m	6.5×10^{-6}
Thickness of the lower polymer (Hormuz Salt)	1.5 mm	Almost welded	
Bulk density of sand / overburden	1500 $kg \cdot m^{-3}$	1900–2650 $kg \cdot m^{-3}$	0.79–0.57
Density of polymer / salt	974 $kg \cdot m^{-3}$	2160 $kg \cdot m^{-3}$	0.45
Angle of internal friction of sand	34.6°	30° to 40°	1–0.6
Viscosity of polymer / salt	1.6×10^{4} Pa·s	10^{17} to 10^{21} Pa·s*	1.6×10^{-15} (average)
Gravitational acceleration	9.807 $m \cdot s^{-2}$	9.807 $m \cdot s^{-2}$	1

et al., 2017). We acknowledge that changes in the salt viscosity affects the horizontal propagation of detachment folding and shortening-triggered diapirism as modelled by Bonini (2003), but this is not the aim of our models. Rather, our aim is to model the effect of contractional deformation on salt structures beyond the thrust wedge and deformation front of Zagros, as seismic data of the study area show an unfolded sedimentary cover containing squeezed salt structures (Hassanpour et al., 2020). Therefore, we shorten the models by less than ~10% in order to avoid any detachment folding or thrusting along the preexisting salt structures (Santolaria et al., 2021) and do not expect to initiate any new salt structure solely by contractional deformation. The 2 mm/3.5 h (0.57 mm/h) of syn-contraction sand deposition in our models corresponds to a sedimentation rate of 34 cm/kyr in nature, in a good agreement with average (compacted) sediment accumulation rates of 18.5–24.7 cm/kyr (Pirouz et al., 2017), 18–52 cm/kyr (Khadivi et al., 2010), 13–42 cm/kyr (Ruh et al., 2014), 35 cm/kyr (Lashgari et al., 2020), and ~12 cm/kyr (Mishan Fm.) and ~63 cm/kyr (Aghajari Fm.) (Najafi et al., 2020) calculated for different Miocene and Pliocene foreland basin deposits of the Zagros.

3.3.3. Physical models visualisation and analysis

The morphometric evolution of the experiments was recorded and subsequently analysed by means of oblique and overhead time-lapse photographs taken every 90 s using computer-controlled high-resolution digital cameras. The same high-resolution cameras were used to record the serial vertical sections carried out at the end of the experiments. The model cross-sections have been obtained by a computer-controlled slicing machine which enabled us to cut the model into 3-mm-spaced sections while simultaneously photographing each cross-section. These cross-sections were used to analyse the along-strike variations in the structures generated in the model. An almost 3-cm-wide section along each side of the experiments was omitted in the analysis to avoid border effects related to the friction between glass side walls and the sandpack (Ferrer et al., 2017; Roma et al., 2018b). Using the serial sections as seeds, we reconstructed the 3D internal architecture of each model and converted it into a 3D pseudo-seismic volume with SEG-Y format (Fig. 4), similar to those of Hammerstein et al. (2014), (Ferrer et al., 2016) or Roma et al. (2018a). This methodology, developed by Hammerstein et al. (2014), allows to convert the photographic data from physical models into seismic SEG-Y volumes and interpret horizons and faults in a seismic interpretation software. This fact, combined with the minimum (3 mm) spacing of the cross-sections at the end of the experiment, allows to build a framework with a huge control of the lateral variability of structures at the same time that new sections in any space direction can be obtained (i.e. dip, strike and oblique sections, or depth slices) (Fig. 4; see also Section 4.3.3).

4. Results

4.1. Seismic interpretation of salt structures

4.1.1. Individual diapirs of Hormuz Salt

Within the studied portion of the Persian Gulf foreland (Fig. 1b), there are two isolated diapirs of the Hormuz Salt, the Lesser Tonb and Namakdan diapirs, where no evidence of Fars-Salt flow is recognised (Fig. 5). The Lesser Tonb diapir is exposed in an island (1 km wide by 1.7 km long) with the same name (Fig. 1b) and it corresponds to a stock of Hormuz Salt (Fig. 5a). Folding and growth geometries of the overburden show that this stock has been squeezed since at least Middle Miocene times (Fig. 5a). As a result, it has been interpreted with a widening upper part regardless of the low resolution of the seismic imaging at the diapir flanks (see also Hassanpour et al., 2020). The wide diapir of Fars Salt east of the Lesser Tonb stock (Fig. 5a) is, in fact, an oblique to strike section of a salt wall peripheral to the Greater Tonb diapir further east

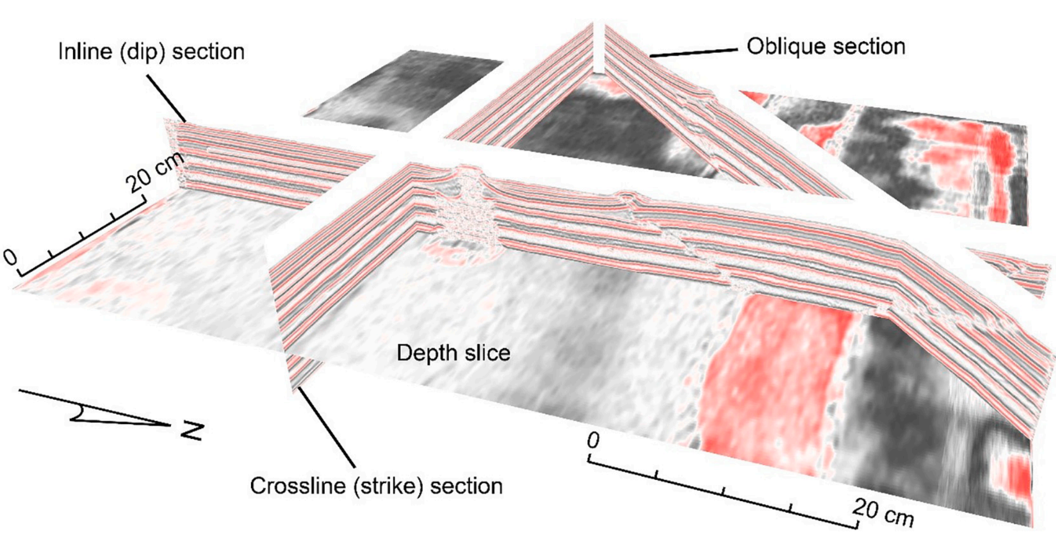

Fig. 4. Oblique view of the pseudo-seismic volume of Model 1 reconstructed from photographs of the serial vertical cross-sections taken at the end of the experiment.

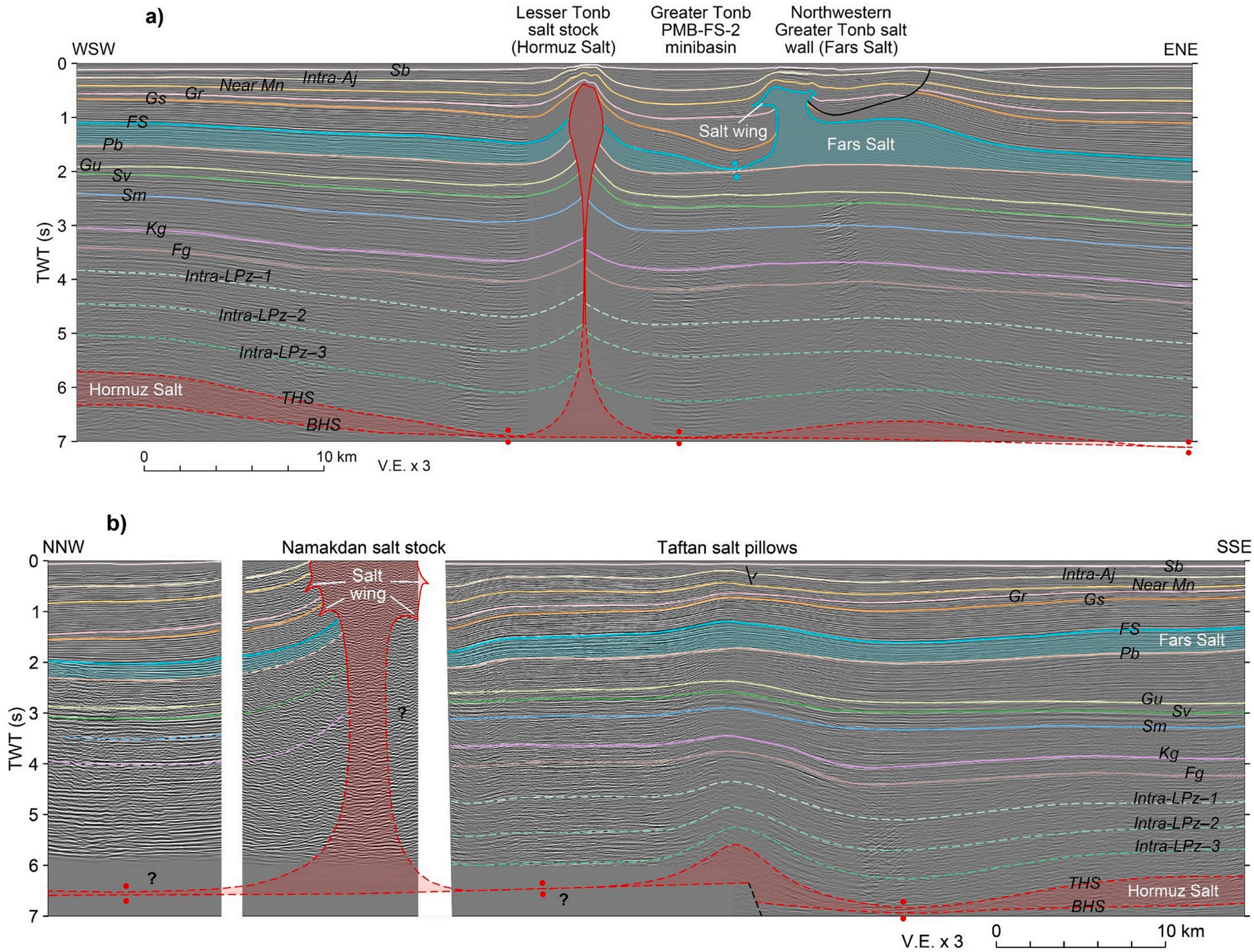

Fig. 5. Interpreted 2D seismic profiles (V.E. x3) across the Lesser Tonb salt stock (a), and the Namakdan salt stock along with the Taftan stacked salt pillows (b). Location of the seismic profiles shown on Fig. 1b. Refer to Fig. 2 for the description of the abbreviated reflectors. Paired red and blue dots denote salt welds related to the evacuation of the Hormuz and Fars salts, respectively. See the text for further details. (For interpretation of the references to colour in this figure legend, the reader is referred to the web version of this article.)

(Fig. 1b). Slight sedimentary thickness variations in the Palaeozoic intervals (Fig. 5a,b) suggest the initiation of the Hormuz-Salt flow and diapirism probably at Cambrian times, soon after salt deposition, even though the quality of the seismic data does not allow the identification of halokinetic sequence geometries related to passive diapirism.

The Namakdan diapir is a circular (~6.5 km in diameter at surface) salt stock exposed in the western part of the Qeshm Island (Fig. 1). Around the outcropping diapir, the Middle Miocene Aghajari Formation strata are upturned into a near vertical (Kent, 1979) to locally overturned (Bosák et al., 1998) attitude showing a collar around the salt contact, with strong bed thinning towards the southeastern edge of the diapir (Player, 1969). Seismic profiles show a flaring upper part of the diapir which suggests its squeezing during the Zagros contractional deformation at Neogene times, although the diapiric stem width is uncertain (Fig. 5b). Slight thinning of the Mesozoic and Cenozoic sedimentary layers is also observed towards the diapir, with few salt wings emplaced in the Neogene layers (Gachsaran, Mishan and Aghajari formations) indicating salt extrusion during its squeezing. At the southern side of the diapir, a thickening of the Middle Miocene Mishan and Aghajari formations towards the diapir likely reflects primary welding of the Hormuz Salt, resulting in depocentre migration towards the diapir (Fig. 5b).

4.1.2. Salt structures related to the interaction of Hormuz and Fars salt horizons

There are clear evidences of significant Fars-Salt flow in three areas in the Eastern Persian Gulf, which include the Abu Musa (Fig. 6), Greater Tonb (Fig. 7), and Hengam (Fig. 8) salt structures. These areas are characterised by salt structures in which the Fars Salt has formed salt walls and anticlines around the Hormuz-Salt diapirs or has risen directly along their edges, suggesting they have dynamically interacted during diapirism. The Abu Musa and Greater Tonb areas have prominent salt walls and anticlines of the Fars Salt around a central diapir fed primarily by the Hormuz Salt (Figs. 6 and 7), whereas Fars-Salt walls are absent around the central Hengam stock (Fig. 8). In these areas, the ring-like array of the Fars-Salt walls and anticlines are flanked by primary welds underlying annular and elongate curved minibasins that contain laterally shifting depocentres (Figs. 6–8).

In these structures, allochthonous salt sheets and wings of the Hormuz Salt were extruded from the central diapir and emplaced in the Pabdeh Formation during Palaeocene–Eocene. Salt extrusion was driven by squeezing of the diapirs during the contractional deformation of the Oman orogenic system to the east (Fig. 1b) (Hassanpour et al., 2020; Snidero et al., 2020). Emplacement of these salt sheets and their subsequent evacuation and welding have resulted in different geometries.

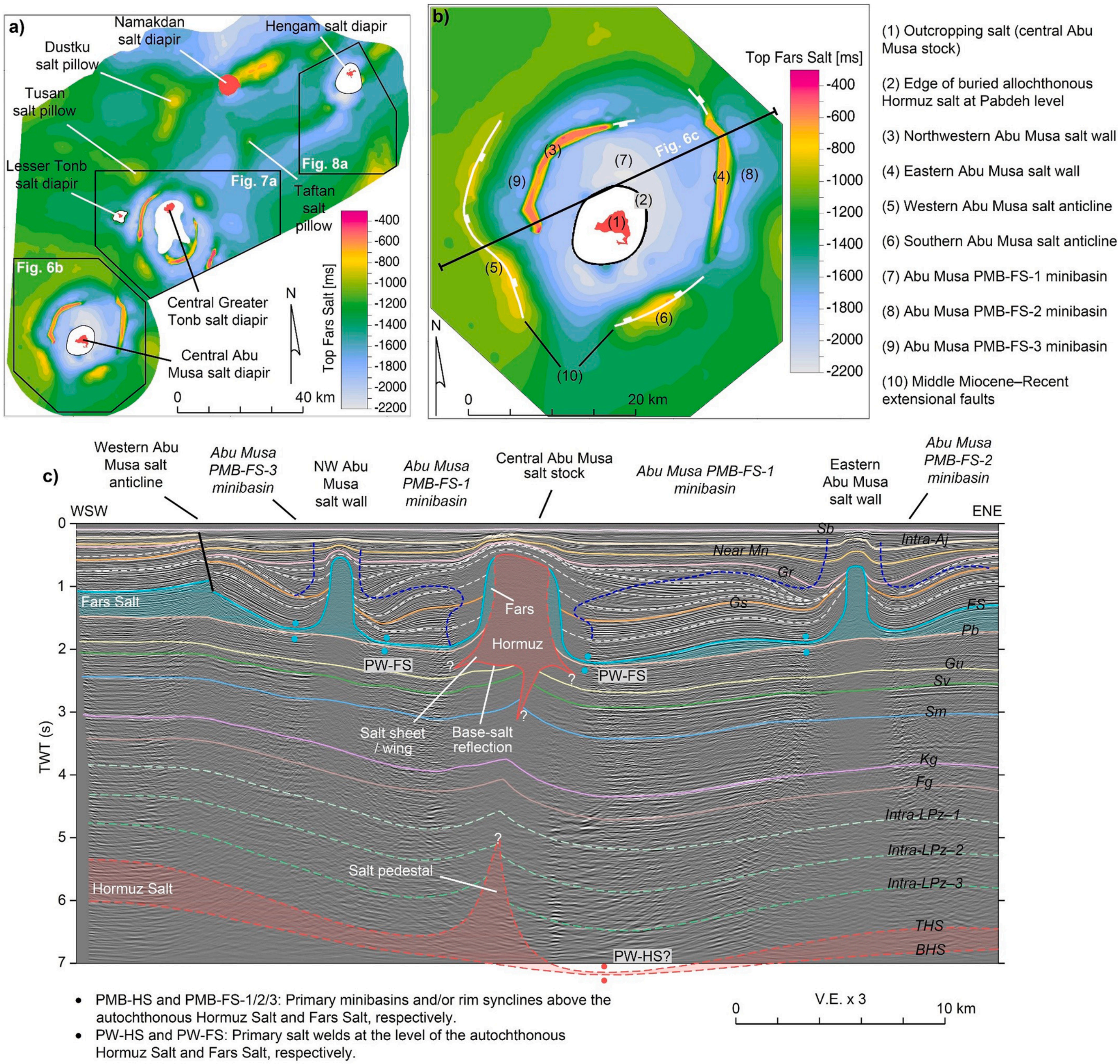

Fig. 6. a) TWT map (in milliseconds) of top Fars Salt in the studied area in the Eastern Persian Gulf, showing the distribution of the salt structures. b) TWT map (in milliseconds) of top Fars Salt around the Abu Musa salt structures; location shown on Fig. 6a. c) Interpreted 2D seismic profile (V.E. x3) across the salt structures in this area. Location of the seismic profile shown on Figs. 1b and 6b. Refer to Fig. 2 for the description of the abbreviated reflectors. Dashed blue lines indicate depocentre axial traces in each minibasin. Paired red and blue dots denote salt welds related to the evacuation of the Hormuz and Fars salts, respectively. See the text for further details. (For interpretation of the references to colour in this figure legend, the reader is referred to the web version of this article.)

For example, tertiary welds have been formed around the Hengam salt diapir (Fig. 8) and likely the Greater Tonb (Fig. 7), but not around the Abu Musa stock (Fig. 6). Allochthonous salt protruding from the Greater Tonb and Hengam central diapirs were also developed at Miocene times, driven by the propagation of the contractional deformation at the Zagros fold and thrust belt front. Two salt sheets were emplaced in the Early Miocene Gachsaran and Middle Miocene Guri intervals around the central Greater Tonb diapir (Fig. 7), and salt wings at least at three levels are recognised in the Guri and Mishan sediments around the Hengam salt stock (Fig. 8) (see also Hassanpour et al., 2020; Snidero et al., 2020). Miocene salt wings are apparently absent from the central Abu Musa salt stock.

The southern part of the central Greater Tonb diapir (Fig. 7) is especially complex as a result of the interaction between the salt structures from both source layers. They have resulted in considerable reduction of the seismic data quality as well as possible velocity pull-ups, and thus have led to two interpretations: an irregular geometry of the central diapir margin flanked by a primary minibasin (Hassanpour et al., 2020), and a secondary minibasin above the diapiric stem (Snidero et al., 2020). With the current data, it is not possible to strongly confirm or reject one of these two scenarios. Whereas SW–NE seismic profiles seem to better support the irregular southern flank of the diapir (Fig. 7b), NW–SE profiles show geometries that are more consistent with a bucket secondary minibasin (Fig. 7c).

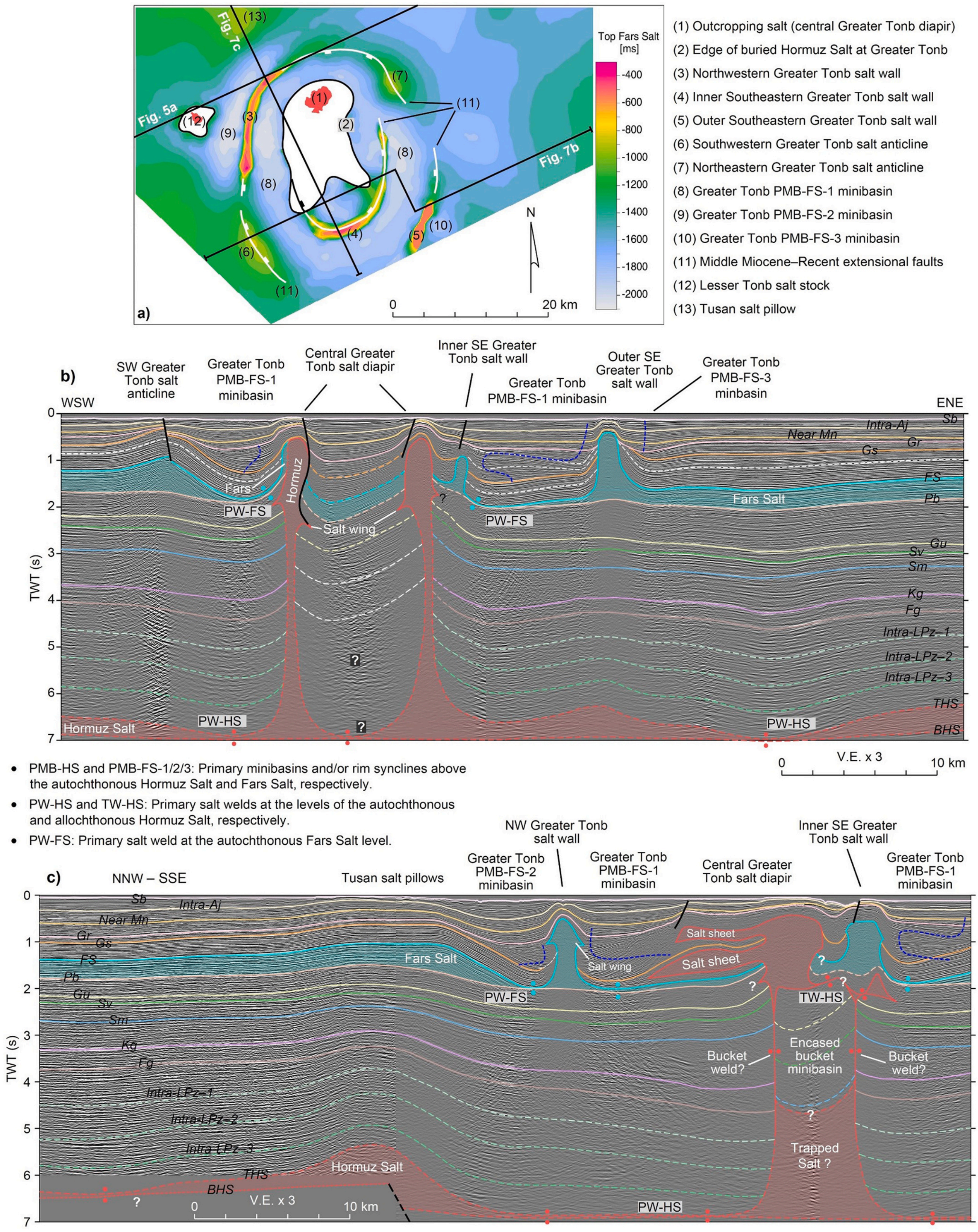

Fig. 7. a) TWT map (in milliseconds) of top Fars Salt around the Greater Tonb salt structures; location shown on Fig. 6a. b) and c) Interpreted 2D seismic profiles (V. E. x3) across the salt structures in this area. Location of the seismic profiles shown on Figs. 1b and 7a. Refer to Fig. 2 for the description of the abbreviated reflectors. Note that the southern part of the central diapir is interpreted as two scenarios: a primary minibasin flanking an irregular salt edge in (b) and a secondary minibasin in (c), as existing data do not allow for constraints on either. Dashed blue lines indicate depocentre axial traces in each minibasin. Paired red and blue dots denote salt welds related to the evacuation of the Hormuz and Fars salts, respectively. See the text for further details. (For interpretation of the references to colour in this figure legend, the reader is referred to the web version of this article.)

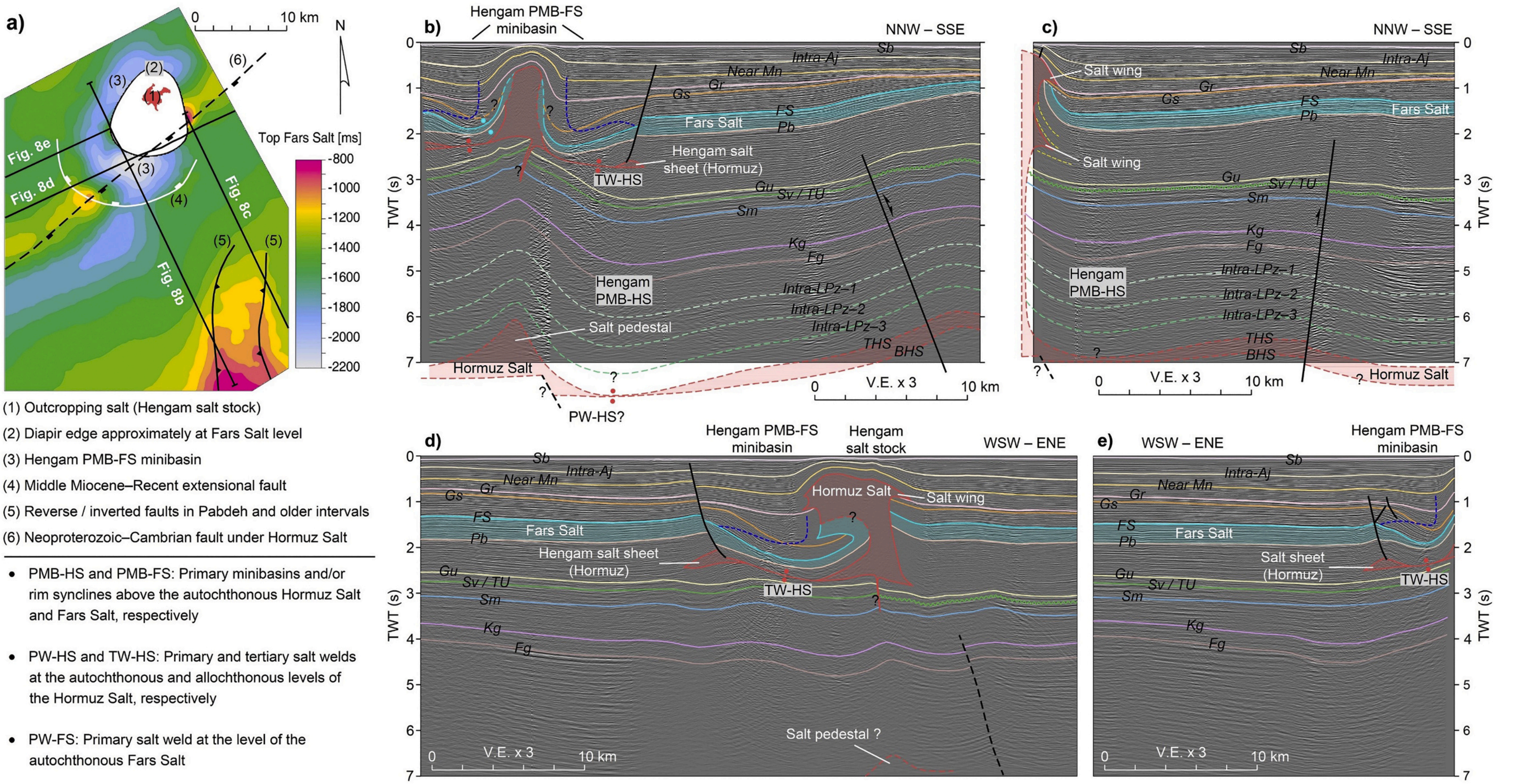

Fig. 8. a) TWT map (in milliseconds) of top Fars Salt around the Hengam salt diapir; location shown on Fig. 6a. b–e) Interpreted 2D seismic profiles (V.E. x3) around the Hengam salt diapir. Location of the seismic profiles shown on Figs. 1b and 8a. Refer to Fig. 2 for the description of the abbreviated reflectors. Dashed blue lines indicate depocentre axial traces in each minibasin. Paired red and blue dots denote salt welds related to the evacuation of the Hormuz and Fars salts, respectively. See the text for further details. (For interpretation of the references to colour in this figure legend, the reader is referred to the web version of this article.)

Detailed seismic interpretation and sequential cross-section restoration suggest that the central diapirs in the Abu Musa, Greater Tonb and Hengam were initiated at Cambrian and subsequently rose as passive diapirs during the Palaeozoic and Mesozoic (Hassanpour et al., 2020; Snidero et al., 2020). These authors also attributed the development of allochthonous Hormuz Salt at Palaeocene–Eocene levels around these diapirs to the squeezing of the diapiric stems by the Oman Mountains contractional deformation. Further younger salt sheets and wings protruded from the same diapirs are also coincident with the final uplift of the Oman Mountains in Late Oligocene–Early Miocene and Zagros

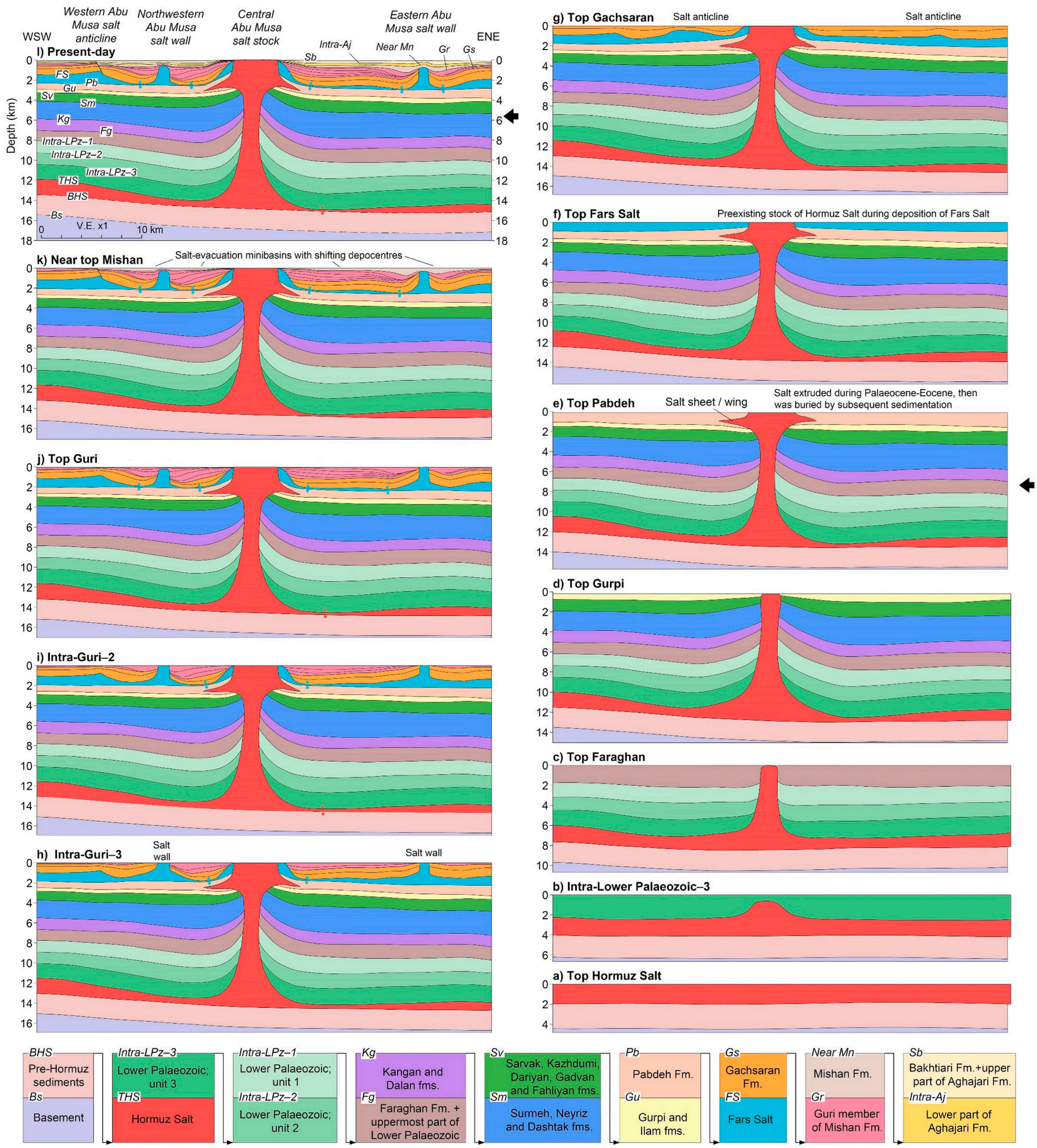

Fig. 9. Sequential kinematic restoration of the Abu Musa salt structures in the Eastern Persian Gulf, carried out using Move software. The Abu Musa area shows one of the three areas in this part of the Persian Gulf where salt flow and diapirism are affected by interaction of the Fars and Hormuz salts structures. Location of the seismic and restored cross-section shown on Fig. 1b. Refer to Fig. 2 for the description of the abbreviated reflectors. Paired red and blue dots denote salt welds related to the evacuation of the Hormuz and Fars salts, respectively. See the text for details and discussions. (For interpretation of the references to colour in this figure legend, the reader is referred to the web version of this article.)

folding since Early–Middle Miocene. These are also concurrent with the initiation of Fars-Salt flow since Early Miocene (see also Jahani et al., 2009; Orang et al., 2018; Ezati Asl et al., 2019; Faghih et al., 2019) and mainly outwards salt flow that formed salt walls and anticlines around these central diapirs (Hassanpour et al., 2020; Snidero et al., 2020). Some of these peripheral salt walls show salt wings extruded into the Middle Miocene sediments during their deposition (Figs. 5–8). These salt walls never reached the seafloor since the deposition of the upper part of the Mishan Formation but are buried under thick arched roofs. It is taken to indicate the welding of the source layer, and the relatively thick arched roof reflects squeezing of the salt walls by the Zagros Neogene contractional deformation during Neogene.

4.1.3. Shallow (Fars Salt) pillows overlying deep (Hormuz Salt) pillows

Gentle salt pillows or salt-cored anticlines involving the Fars Salt are observed above deep-seated Hormuz-Salt pillows, such as the Taftan, Tusan, and Dustku ones (Figs. 5 and 7). These structures are the best ones to decipher the earliest movement of the Hormuz Salt because of the good quality of the seismic imaging of the overburden. Thinning of the overburden strata above the Hormuz-Salt pillows suggests inception of salt inflation at Cambrian times, immediately or shortly after its deposition (Figs. 5 and 7) (Hassanpour et al., 2020; Snidero et al., 2020). These pillows were growing at Early Palaeozoic but their rise slowed down towards the end of Palaeozoic, and were almost inactive under thick roofs during the Mesozoic. These inactive salt pillows were subsequently rejuvenated during Palaeocene–Eocene and Miocene–Recent contractional deformation events related to the Oman and Zagros orogenic belts. The Fars Salt shows evidence of minor inflation above the thick roof of these deep Hormuz-Salt pillows since the deposition of the Early Miocene Gachsaran Formation (e.g. Taftan and Tusan pillows in Figs. 5b and 7b). The mechanism driving the growth of these shallow pillows was differential loading accompanied synchronously by the Zagros folding (Hassanpour et al., 2020; Snidero et al., 2020).

4.2. Sequentially restored cross-section

A cross-section along the seismic profile of Fig. 6 has been restored aiming to illustrate the structural evolution of the Abu Musa salt structures (Fig. 9) (see also Hassanpour et al., 2020). This section has been shifted southwards at the location of the central salt stock to cross its axis, in order to include the interpreted geometry of the diapir stem even though its width is uncertain. The restoration illustrates that the Hormuz Salt with a reconstructed thickness of ~2 km (Fig. 9a) began flowing at about Cambrian times forming the incipient Abu Musa salt pillow (Fig. 9b). Salt reached the depositional surface (or just beneath it) probably very soon by pressurised flow due to differential sedimentary loading and a passive diapir rose continuously throughout the Palaeozoic and Mesozoic. (Fig. 9b–d).

During deposition of the Palaeogene Pabdeh Formation, contractional deformation at a horizontal rate of 1–2 mm/yr (Hansman et al., 2017) related to the Oman Mountains to the east led to the layer-parallel shortening of the sedimentary sequence in the Eastern Persian Gulf. It resulted in the squeezing of the Abu Musa salt stock and extrusion of an allochthonous body of Hormuz Salt that was buried by younger sediments of the Pabdeh Formation (Figs. 6 and 9e) (Hassanpour et al., 2020). This was followed by deposition of the Fars Salt at the Oligocene–Early Miocene (Fig. 9f).

The Fars Salt began flowing during deposition of the Gachsaran Formation, resulting in the formation of salt walls and anticlines around the Hormuz-Salt stock; some of the Fars Salt flowed towards the central stock and rose along its margins (Fig. 9g,h). Evacuation of the Fars Salt during deposition of the basal part of the Middle Miocene Guri member promoted primary welding (Fig. 9h) and the development of salt-evacuation minibasins containing laterally shifting stacked depocentres (Fig. 9i–l), similar to expulsion rollover structures (Ge et al., 1997). Salt structures (central stock and peripheral salt walls) were also rejuvenated by the Zagros contraction, leading to the final emergence of the Hormuz Salt in the Abu Musa Island and arching the Miocene and Pliocene roof strata above the Fars-Salt walls surrounding the stock (Fig. 9l).

4.3. Results of physical models

4.3.1. Model 1 evolution

Shortening started after deposition of a pre-contractional blue sand layer above the upper (green) polymer (Figs. 3c,d and 10a,b). During the first ~20 mm of shortening, the sandpack was horizontally compacted due to porosity reduction, with the layer-parallel shortening being the major component of deformation (Koyi et al., 2004; Burberry, 2015), without the development of any macroscale contractional structures such as folds and thrusts. This layer-parallel shortening was enough to squeeze and rejuvenate the buried salt stock, gradually arching and uplifting its roof (Fig. 10c). In addition, shallow-rooted structures developed along (or few millimetres away from) the inner pinch-out of the upper polymer. The top of the stock rose above regional and the salt body was translated towards the foreland (Fig. 10c).

After 42 mm of shortening, incipient deep-seated fore- and backthrust faults dipping ~30° and bounding a broad boxfold anticline were initiated at the hinterland of the model, far from the salt structures (Fig. 10d). At this stage, the two deep-rooted thrust structures practically have not yet surface expressions; rather two shallow thrusts formed along the backlimb of the boxfold anticline. Further shortening up to 72 mm allowed the upwards propagation of the deep-rooted thrusts and additional squeezing of the salt stock (Fig. 10e,f). As a result, growth and uplift of the main boxfold anticline above the incremental regional datum resulted in the shifting of the sedimentation area to the foreland. A progressive offlap of the syn-contractional sand layers against the backlimb of the boxfold anticline is observed.

The lower (blue) polymer at the centre of the stock pierced the stretched roof after 63 mm of shortening and extruded to form overhangs until the end of the experiment (Fig. 10e,f). This was accompanied by the rise and extrusion of the upper polymer around the edges of the lower polymer stock (Fig. 10f). The deep-rooted backthrust reached the surface, whereas the forethrust was either detached upwards along the upper polymer or coincided with the shallow-rooted structure at the inner pinch-out of the upper polymer. The deformation front at the end of the experiment did not reach the salt stock but the final position of the stock shows a horizontal translation of ~20 mm towards the foreland (Fig. 10f).

4.3.2. Model 2 evolution

In Model 2, in contrast to Model 1, a pure gravitational loading (downbuilding) episode was imposed on the upper (green) polymer before shortening (Fig. 11a,b). The ring-shaped removal of the blue sand layer directly overlying the upper polymer created a differential sedimentary load that led to rise of the polymer to the depositional surface (Fig. 11b). Salt rise along the annular wall was balanced by sinking into the polymer of surrounding minibasins, accommodating the syn-halokinesis sand layers and leading to polymer expulsion into the salt wall as well as towards the central stock margin.

As in Model 1, the onset of regional contraction led to layer-parallel shortening of the sandpack without the development of any macroscale structures (Koyi et al., 2004; Burberry, 2015), but started to rejuvenate the annular salt wall and the dormant central stock (Fig. 11c). Further contractional deformation is characterised by continuous uplift of the central stock and annular salt wall polymers, as well as roof arching and stretching (Fig. 11d). Roof stretching triggered the development of radial and longitudinal extensional faults above the stock and along the annular salt wall, respectively (Fig. 11d). These structures also represent forelandwards translation due to shortening. At this stage, few shallow-rooted thrusts were also nucleated along the inner pinch-out of the upper polymer (Fig. 11d). The addition of syn-contractional

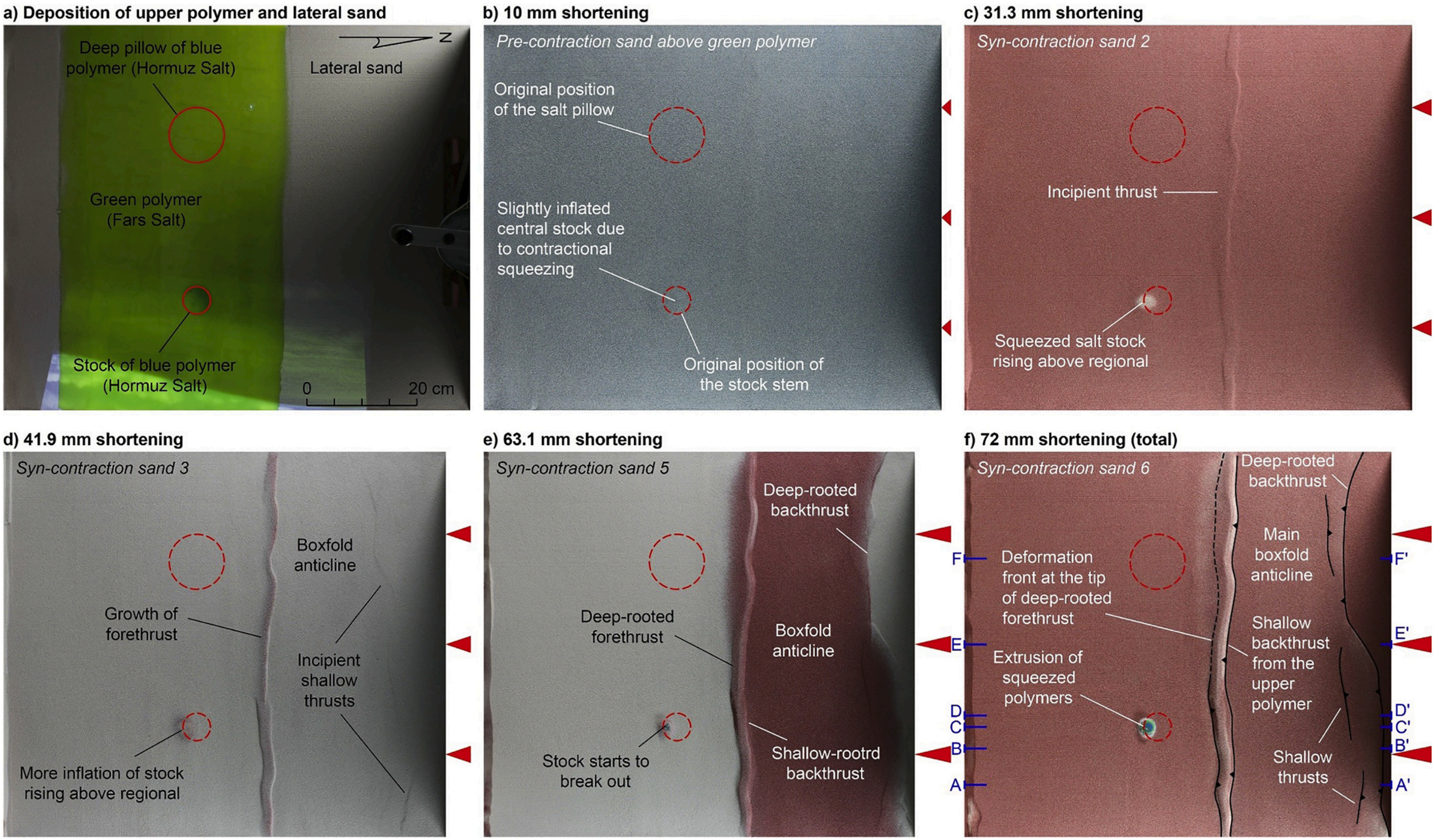

Fig. 10. Overhead pictures showing the evolution of Model 1. a) Experimental configuration after the deposition of the upper polymer layer (green) simulating Fars Salt. b) Configuration after the deposition of the last pre-contractional sand layer. c–f) Overhead evolution during model shortening. (For interpretation of the references to colour in this figure legend, the reader is referred to the web version of this article.)

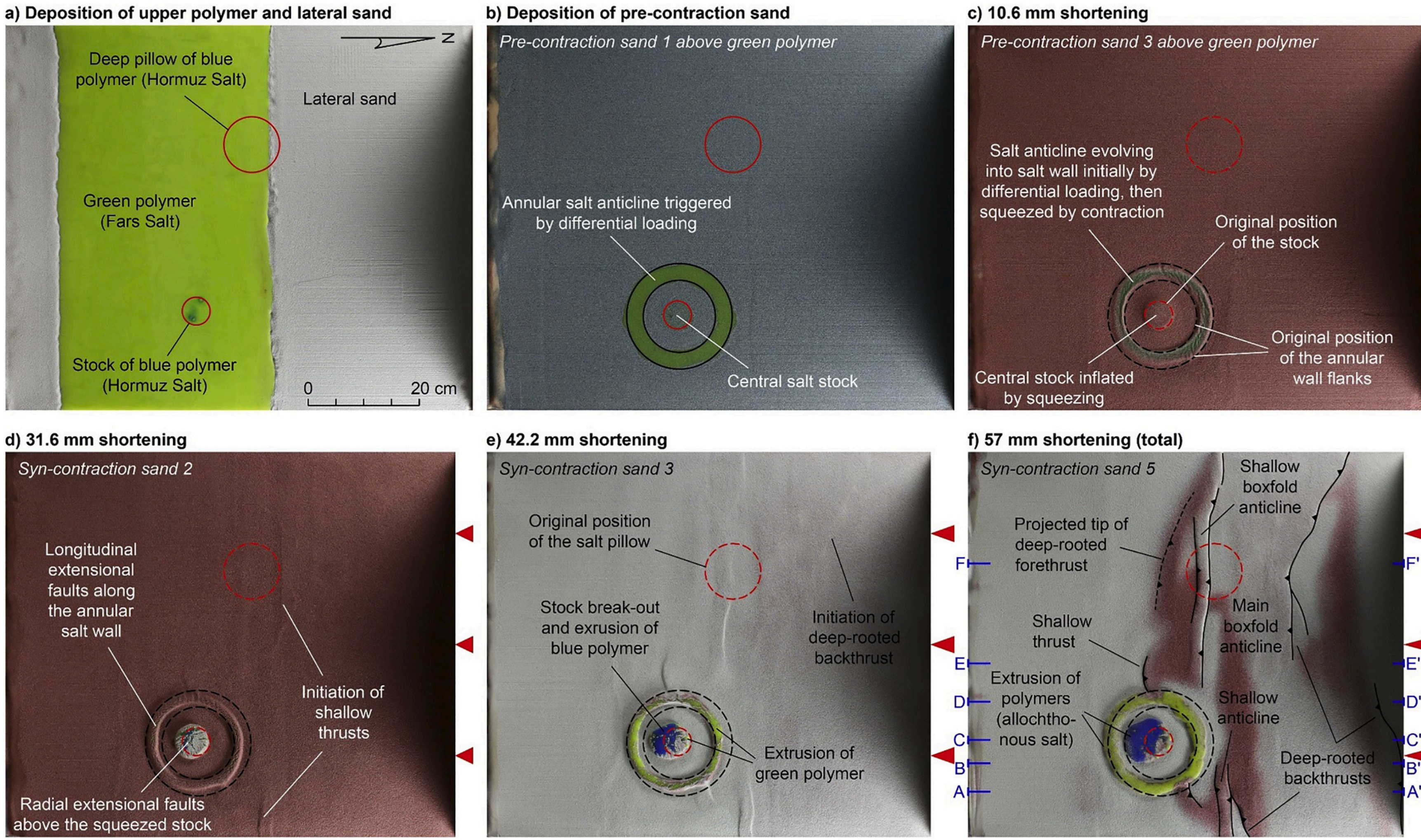

Fig. 11. Overhead pictures showing the evolution of Model 2. a) Experimental configuration after the deposition of the upper polymer layer (green) simulating Fars Salt. b–c) Evolution of the experiment during the gravitational loading (downbuilding) stage. d–f) Overhead evolution during model shortening. (For interpretation of the references to colour in this figure legend, the reader is referred to the web version of this article.)

sedimentation enhanced the sinking of the minibasins surrounding the annular salt wall and the salt stock. This occurred coevally to contractional squeezing and both processes together maintained the polymer uplift up the diapirs, leading to salt extrusion (Fig. 11e).

During shortening the model from 32 mm (Fig. 11d) to 42 mm (Fig. 11e), two broad boxfold anticlines bounded by two incipient ~25–30° dipping fore- and backthrust faults occurred in the hinterland. The previously formed shallow-rooted thrusts detached in the upper polymer continued to grow. The central salt stock and the annular wall pierced through their thinned and dismembered roof and polymer started lateral extrusion above the surrounding sand (Fig. 11e). From this point onwards, the two main boxfold anticlines were quite developed in the hinterland. The western anticline (north pointing to the backstop) formed above the deep-seated salt pillow, whereas the eastern one occurred behind the salt stock (Fig. 11f). The deep-rooted backthrusts breached the surface, whereas the forethrust was terminated upwards into the upper polymer. Uplift of the boxfold anticlines above regional datum is characterised by thinning of sand layers towards the crest of the structures and shifting of depositing sand towards the foreland. The diapirs continued extruding polymer above the surrounding sand, forming salt sheets. At the end of the experiment, the diapirs show a ~20 mm translation towards the foreland (Fig. 11f).

4.3.3. Serial vertical cross-sections and depth slices

The study of model surfaces during their evolution (Figs. 10 and 11) and the pseudo-seismic volumes discovering their final internal structures (Figs. 12–15) reveal that the main boxfold anticlines and bounding fore- and backthrusts have been transported towards the foreland in the western part of both models. At the basal parts of the structures, this shift measures by ~7 and ~15 cm in Model 1 (Fig. 14d) and Model 2 (Fig. 15d), respectively. Differences are sharp such that the boxfold was nucleated at the salt pillow in Model 2 (Fig. 15), whereas formed behind the pillow in Model 1 (Fig. 14). This led to a relay between the boxfolds in Model 2. These boxfolds also show a shorter wavelength in the salt pillow parts of both models. In Model 1, the boxfold is a more linear structure at surface (Fig. 14a), whereas at depth it splays from west to east into two different branches (Fig. 14c,d). The southern branch dies out laterally, suggesting that the final boxfold structure could result from two relay boxfolds that eventually merged as shortening increased. Another important observation is that the deep salt pillow has been translated towards the foreland in both models (Figs. 14 and 15). However, the pillow was only slightly deformed during shortening of Model 1 (Fig. 14d), whereas its circular shape has been clearly deformed in Model 2, acquiring an elliptical shape with the larger axis orthogonal to the shortening direction (Fig. 15d) and nucleated the boxfold in Model 2 (Fig. 13), despite considering that Model 2 was shortened 15 mm less than Model 1. We attribute this difference of deformation to the distance of the salt pillow from the deformation backstop, which was by 10 cm shorter in Model 2 compared to Model 1 (see Fig. 3a,b). Therefore, the pillow was closer to the deformation front in Model 2 and the contractional strain was concentrated in the weak pillow and nucleated the boxfold above it. On the contrary, the pillow in Model 1 was only affected by layer-parallel shortening and transported towards the foreland. These results suggest the control of salt structures on the location and wavelength of large-scale contractional structures developed during shortening (Jahani et al., 2009; Callot et al., 2012; Duffy et al., 2018; Hassanpour et al., 2018; Santolaria et al., 2021). While on one hand the pillow is located in a position that favours the nucleation of the boxfold for the specific thickness of the overburden, on the other hand, the diapir that is located further away from the moving wall, is not used as a nucleation point of the boxfold for the thickness of the cover (Figs. 12–15).

The main deep-rooted backthrust along the backlimb of the anticline has approximately a constant average dip across each model, whereas the forethrust shows a shallower dip upwards as it approaches the upper polymer. The change is dramatic where the upper tip of the forethrust meets the upper polymer along its inner pinch-out (i.e. in Model 1; Fig. 12). On the contrary, in Model 2, the upwards decrease in the forethrust dip is seen in the eastern part of the model where the fault tip terminates at or near the inner pinch-out of the upper polymer (Fig. 13). At the western part of this model, where there is a strong shift of the boxfold and bounding thrusts towards the foreland (Fig. 15), the forethrust dip is constant (Fig. 13). Both models have also shallow thrust faults and their corresponding detachment anticlines along or near the inner pinch-out of the upper polymer. In both models, the northern shallow thrust is extended almost everywhere but the southern shallow thrust is more local and segmented.

5. Discussion

5.1. Triggering of Fars Salt flow

The structures of the Fars Salt are systematically associated with the preexisting Hormuz-Salt structures (Fig. 1b), either in form of gentle salt pillows above deep-seated pillows, or as salt walls and anticlines around some of the preexisting diapirs (Figs. 5–8). This suggests that there has been a close genetic relationship between the presence of the Hormuz-Salt structures, existing since Cambrian, and Fars Salt evacuation–inflation processes after its deposition at Oligocene–Early Miocene times. In addition, the Hormuz-Salt diapirs around which the Fars Salt has been evacuated (Abu Musa, Greater Tonb, and Hengam) have extruded allochthonous Hormuz Salt forming salt sheets and wings at Palaeocene–Eocene and Miocene times, some of which were later evacuated (Figs. 6–8) (see also Hassanpour et al., 2020; Snidero et al., 2020). Conversely, Fars-Salt anticlines and walls are absent around other nearby stocks of the Hormuz Salt (e.g. Namakdan and Lesser Tonb stocks) despite the presence of a ~650–950-m-thick Fars Salt around them (Fig. 5). Around these stocks, the presence of allochthonous Hormuz Salt is limited to few small salt wings within Miocene deposits adjacent to the Namakdan salt stock. The Namakdan and Lesser Tonb stocks exemplify a squeezed geometry with a flaring upper part in the Cenozoic intervals. This suggest that the Namakdan and Lesser Tonb stocks had relatively thick roofs during Palaeocene–Eocene, so that the salt pressurised by regional shortening could have only arched the roof without extrusion of evaporites, similar to the shortened thick-roof diapirs in the physical models (Vendeville and Nilsen, 1995; Duffy et al., 2018).

The Fars Salt began flowing during deposition of the Gachsaran Formation (Early Miocene) when contractional deformation was active in the Oman Mountains at Late Oligocene–Early Miocene times. On the other hand, there are evidences that differential sedimentary loading was a very influential driving force for the salt movement and diapiric growth of the Fars Salt during Neogene contractional deformation of Zagros. Therefore, the question is what triggered Fars-Salt mobilisation: differential sedimentary loading (gravitational loading) or regional shortening? Our physical modelling results have some clues to answer this question.

In the physical Model 1, where no differential sedimentary loading was imposed on the upper polymer analogous to the Fars Salt, the polymer layer remained practically undeformed except for local salt inflation exactly at the margin of the rising salt stock made of the Hormuz-Salt equivalent polymer. Thus, no isolated salt structures were developed from the shallow polymer that was affected by shortening until the end of experiment (Figs. 10 and 12). Conversely, in Model 2, early gravitational loading of the upper polymer triggered the formation of an inflated salt zone that grew into a salt wall before the onset of contraction (Figs. 11 and 13). The initial flow of the Fars Salt took place at Early Miocene that was synchronous with the Late Oligocene–Early Miocene contractional deformation and uplift of the Oman Mountains to the east or the Early Miocene inception of the Zagros folding to the north. However, seismic interpretation of the Fars-Salt overburden geometries combined with the restored cross-section and presented

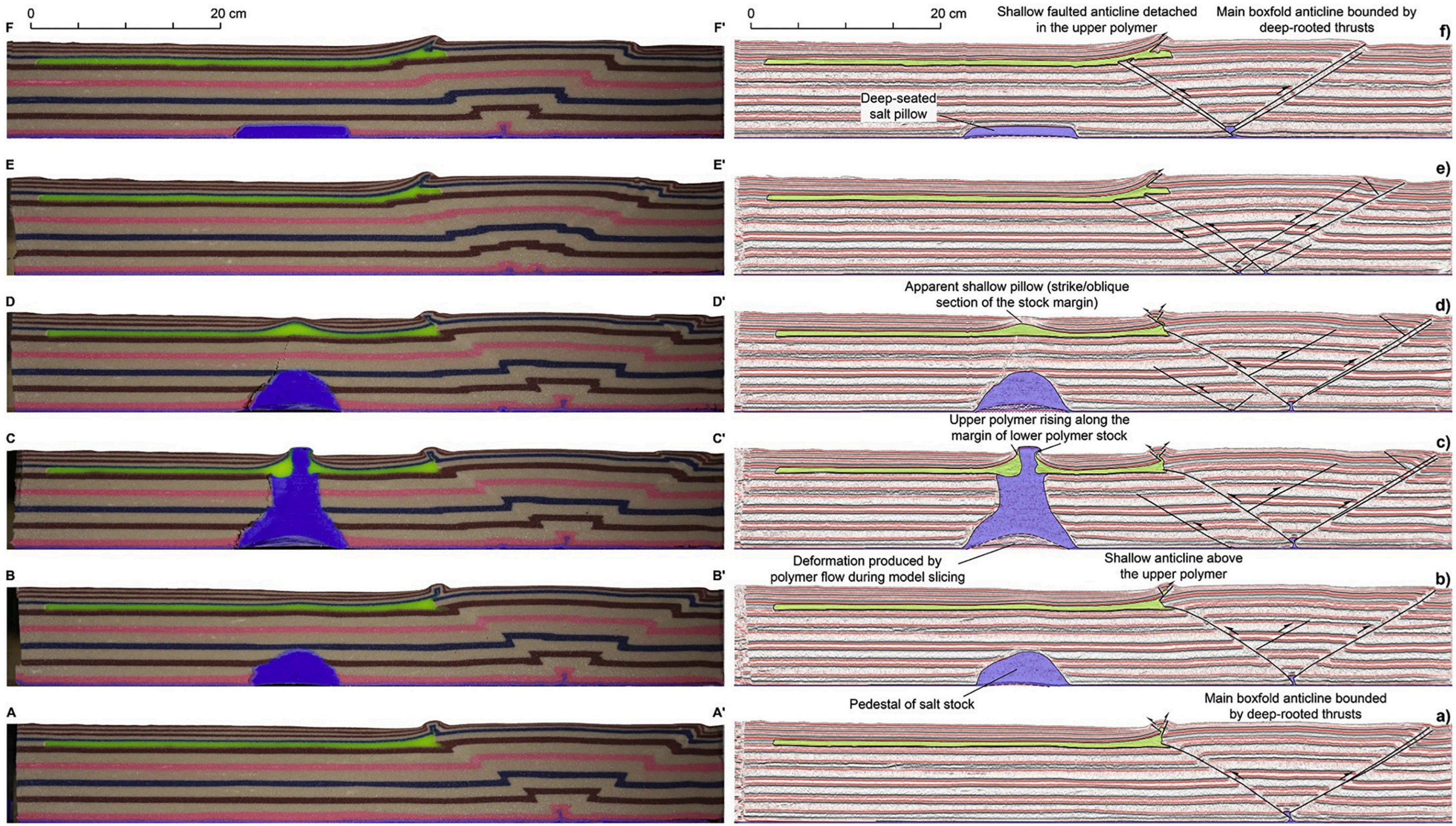

Fig. 12. Uninterpreted (left) and interpreted (right) serial cross-sections of Model 1 at the end of the experiment. See Fig. 10f for the location of cross-sections.

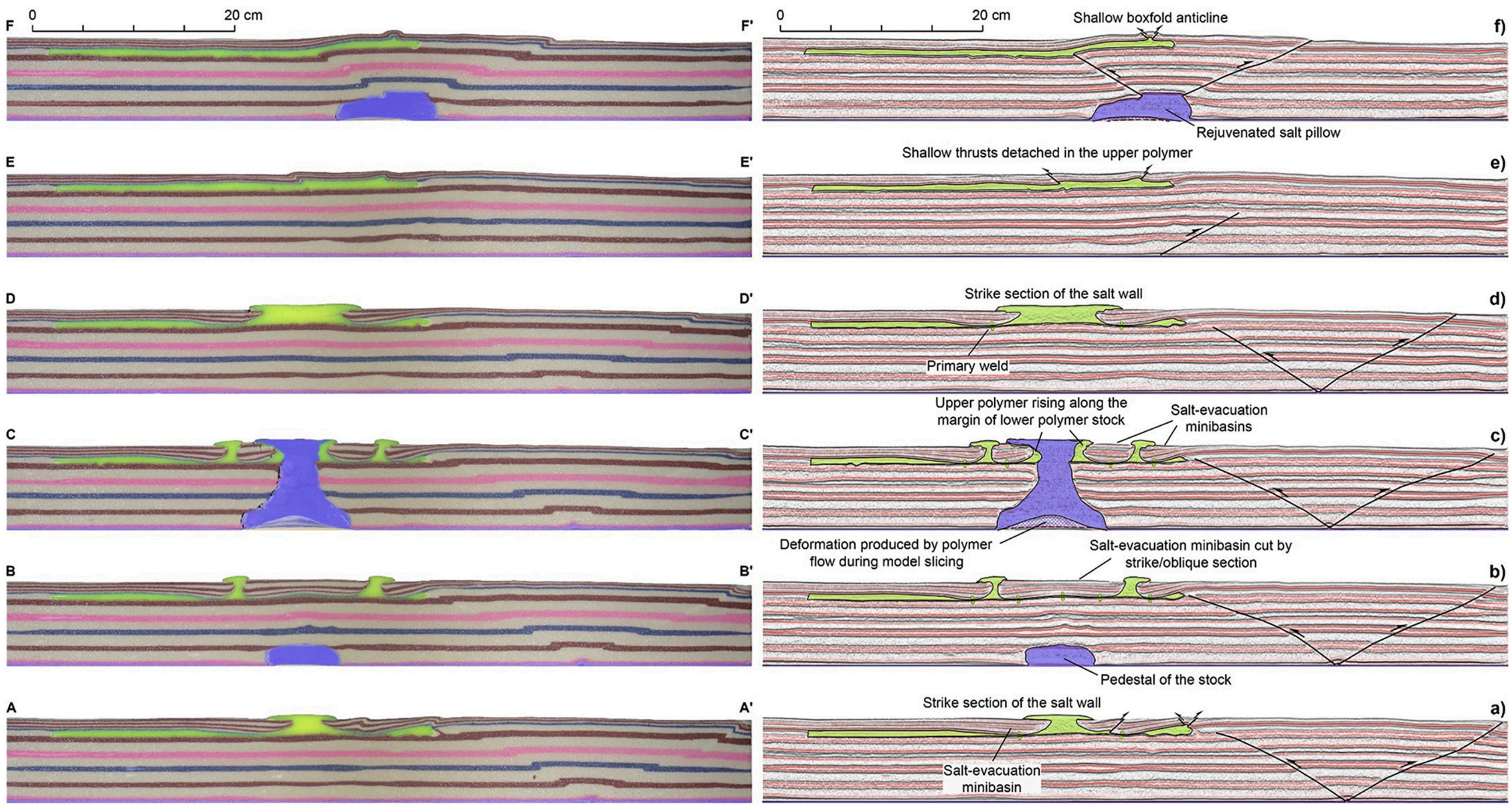

Fig. 13. Uninterpreted (left) and interpreted (right) serial cross-sections of Model 2 at the end of the experiment. See Fig. 11f for the location of cross-sections.

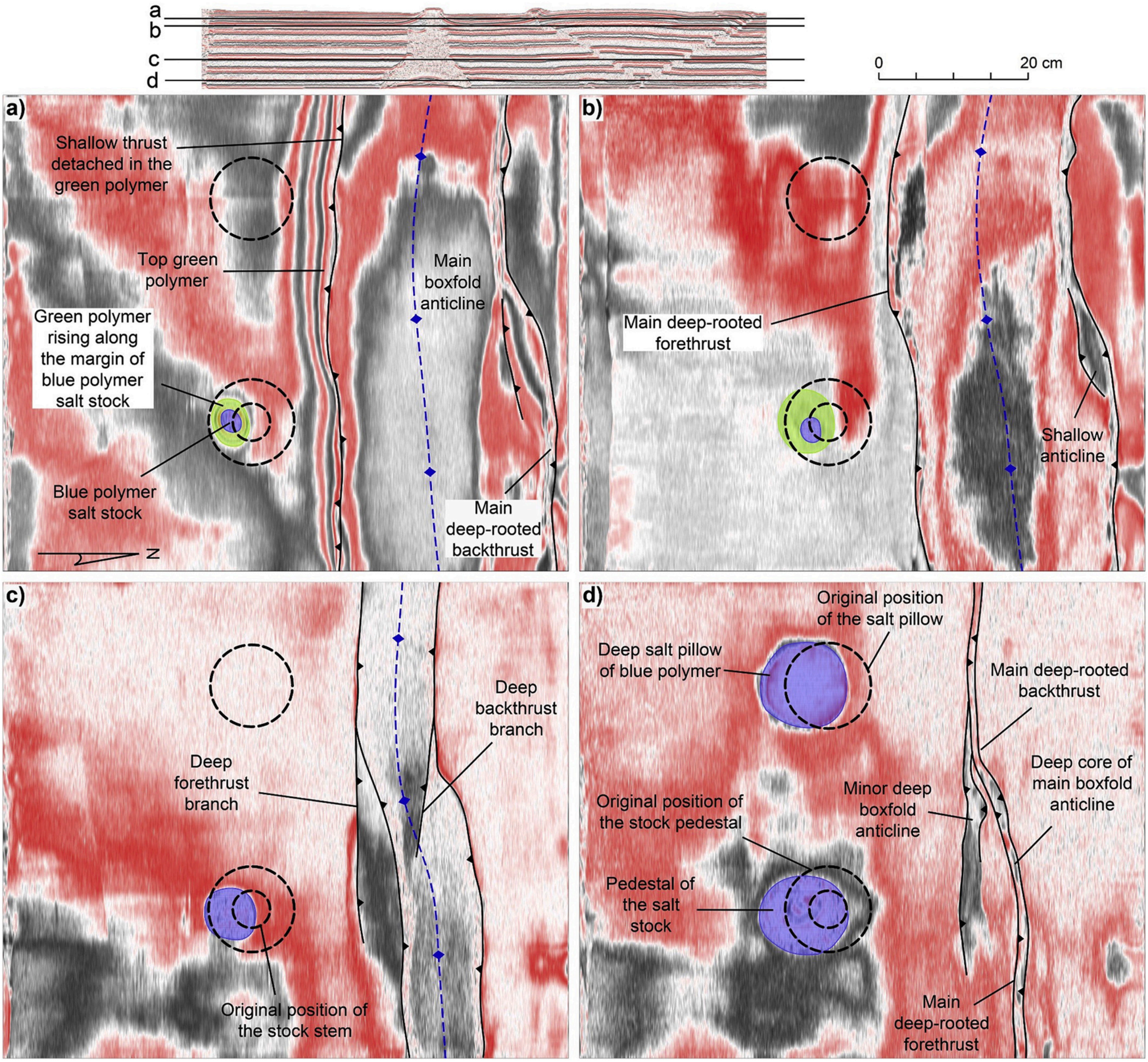

Fig. 14. Depth slices extracted from seismic volume reconstructed from the serial cross-sections of Model 1 at the end of the experiment.

experimental observations suggest that the prime mechanism in triggering the Fars-Salt flow was differential sedimentary loading as the evidence of the main phase of regional shortening in the area is younger than the time of initial salt flow. Therefore, shortening was more influential subsequently during contractional rejuvenation and squeezing of the salt structures mainly since Late Miocene. Now, the question is what could be the cause of the differential load?

Dooley et al. (2012) present physical models showing that a deeper allochthonous salt sheet can be subsequently expelled laterally under a differential load imposed by an overriding shallower salt sheet. Referring to this work, Snidero et al. (2020) propose that the development of a major allochthonous Hormuz-Salt sheet from the central Greater Tonb diapir shortly after Fars Salt deposition (Fig. 7b) exerted a differential load on the Fars Salt and triggered its lateral flow. Although we agree with the role of this salt sheet in the Greater Tonb area, its absence in the Early Miocene level around the central Abu Musa and Hengam diapirs (Figs. 6 and 8) may suggest another more general mechanism in triggering the Fars-Salt flow around the Hengam, Greater Tonb, and Abu Musa central diapirs. A common characteristic of these three salt structures is the Palaeocene–Eocene extrusion of Hormuz Salt and its emplacement in the middle part of the Pabdeh Formation, forming allochthonous salt bodies with variable lateral extents (i.e. salt sheets and wings) (Figs. 6–8). Taking these points, we suggest that the initial flow by the early differential load on top of the Fars Salt was more likely triggered by the generation of pressure and elevation head gradients (Fig. 16a1–2, b1–2) due to evacuation or rearrangement of the allochthonous Hormuz Salt emplaced before the deposition of the Fars Salt (Figs. 6–9). In this model, evacuation of these Hormuz-Salt sheets and wings was triggered by differential loading resulting from deposition of the Gachsaran Formation or even older sediments (the Fars Salt itself) overlying the salt sheet or wing (see also Hassanpour et al., 2020; Snidero et al., 2020). Post-emplacement evacuation of salt wings and sheets by vertical loading caused by younger overlying sediments has also been documented in seismic data from other salt basins such as the

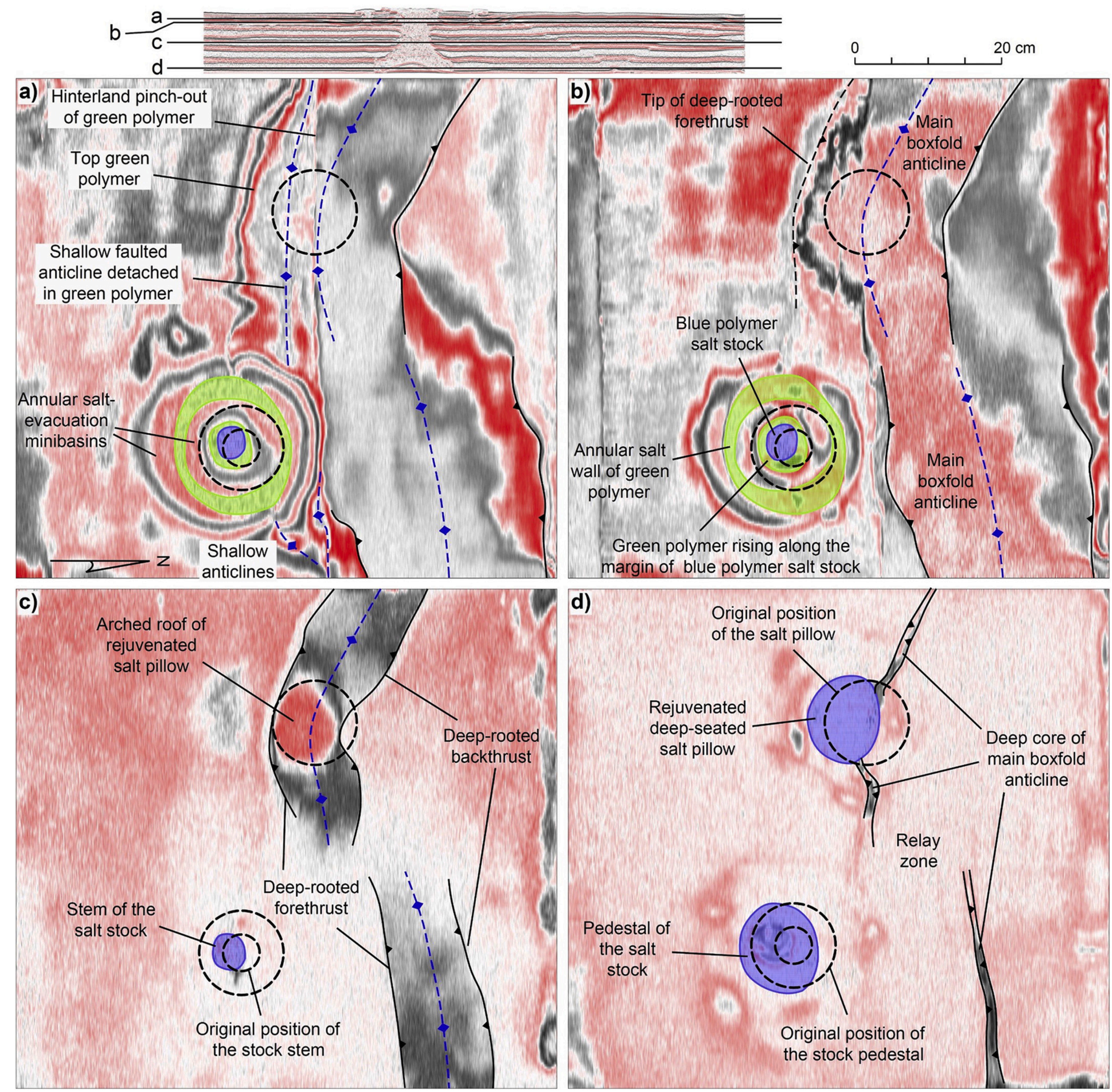

Fig. 15. Depth slices extracted from seismic volume reconstructed from the serial cross-sections of Model 2 at the end of the experiment.

Gulf of Mexico (Jackson and Hudec, 2017).

5.2. Fars Salt evacuation and development of salt structures

Once the Fars Salt started to flow laterally, the expelled salt either created isolated salt anticlines around some of the diapirs of Hormuz Salt (Abu Musa and Greater Tonb) (Figs. 6, 7 and 9), or flowed inwards to coalesce with the edges of these preexisting diapirs (Figs. 6–9 and 16). The latter occurred in all three areas (Abu Musa, Greater Tonb, and Hengam) but was most effective in the Hengam area where there is no peripheral isolated walls of Fars Salt around the central stock (Fig. 8). In the Abu Musa and Greater Tonb, the incipient inner salt anticlines were progressively inflated by the evacuation of Fars Salt from both sides (Fig. 9g), resulting in their conversion into salt walls (Fig. 9h). In contrast, the outer salt anticlines never evolved into salt walls although they were subsequently cut by longitudinal extensional faults due to collapse of the flank that faces towards the central diapir (Figs. 6, 7 and 9h–l).

The extent of the Palaeocene–Eocene allochthonous salt bodies decreases westwards from Hengam to Greater Tonb and Abu Musa (Figs. 6–8). It is known that the diapir shape (stock vs. wall) (Callot et al., 2007; Jackson and Hudec, 2017; Hassanpour et al., 2020; Santolaria et al., 2021), the width (narrow vs. wide) (Nilsen et al., 1995; Vendeville and Nilsen, 1995) and dip of diapiric stems (vertical vs. leaning) (Dooley et al., 2015; Santolaria et al., 2021), the diapir roof thickness prior to shortening (Dooley et al., 2015; Duffy et al., 2018; Santolaria et al., 2021), diapir location with respect to the structural spacing (Callot et al., 2012; Santolaria et al., 2021), as well as the

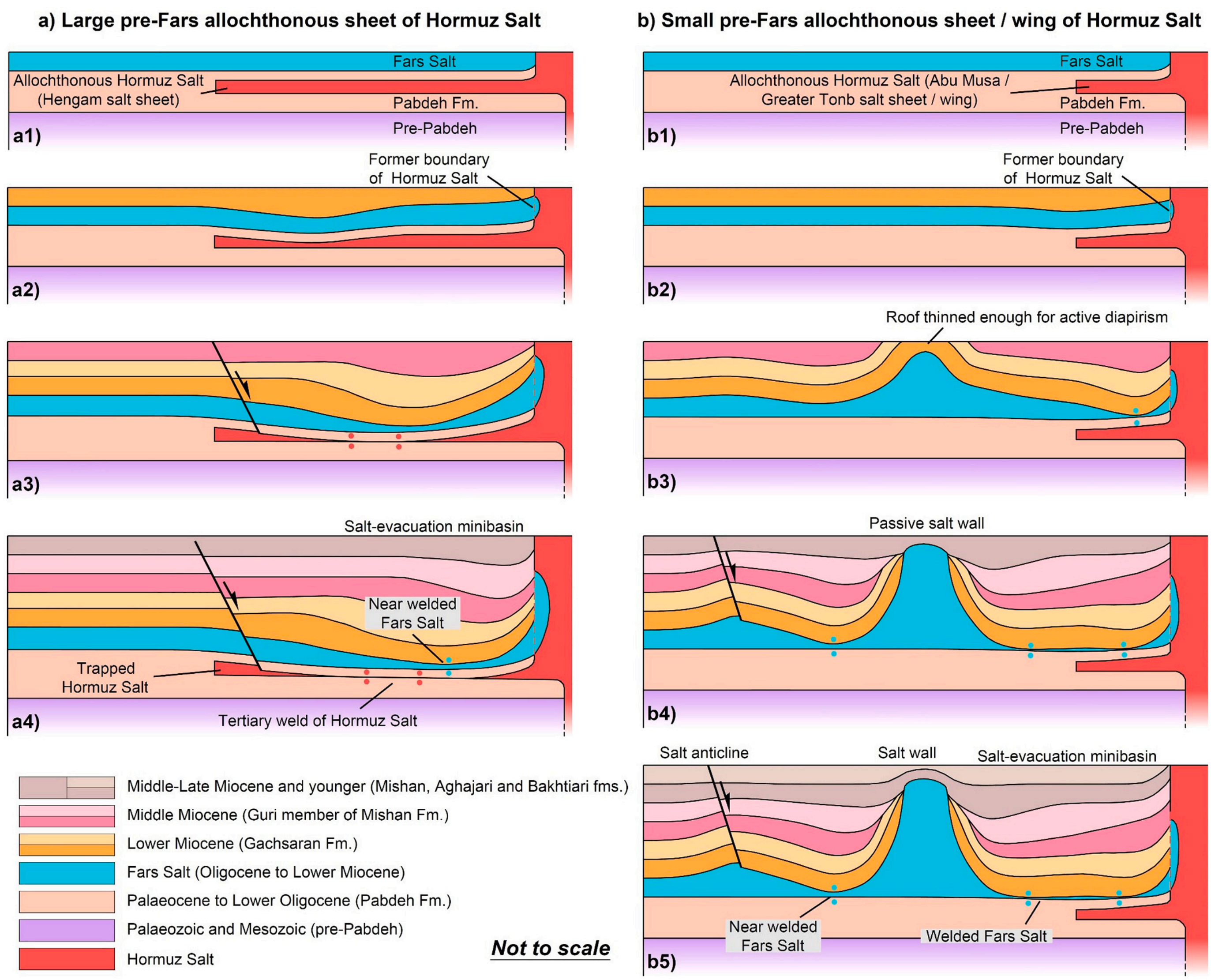

Fig. 16. Simplified schematic forward model cartoons summarising the proposed kinematics of Fars-Salt flow and diapirism in the Eastern Persian Gulf. No compaction was taken into account. The models highlight the relationship between gravitational differential loading of underlying allochthonous bodies of the Hormuz Salt emplaced at Palaeocene–Eocene level and flow of the Fars Salt. a) Flow of the Fars Salt where the underlying salt sheet is laterally large and is extensively evacuated (i.e. Hengam area). The Fars Salt flowed inwards to coalesce with the edge of the preexisting diapir of Hormuz Salt. b) Flow of the Fars Salt where the underlying salt sheet is laterally small and only slightly evacuated or rearranged (i.e. Abu Musa and Greater Tonb areas). The Fars Salt flowed mainly inwards at the early stage to coalesce with the edge of the preexisting diapir of Hormuz Salt, followed by outwards flow to feed the isolated salt wall of the Fars Salt. See the text for details and discussions. (For interpretation of the references to colour in this figure legend, the reader is referred to the web version of this article.)

orientation of salt walls with respect to the shortening direction (Dooley et al., 2009b; Duffy et al., 2018) control the deformation of salt diapirs during lateral contraction. The Abu Musa, Greater Tonb, and Hengam central diapirs are vertical diapirs (Figs. 6–8), but the other mentioned factors are still unconstrained. Therefore, we argue that the larger salt sheet at the Hengam diapir compared to the Abu Musa and Greater Tonb could be largely related to the closer position of the Hengam diapir to the Oman–Zagros deformation front as it progressed from hinterland towards the foreland (Fig. 1a), hence its larger degree of squeezing. As a result, the allochthonous salt emplaced in the Palaeogene Pabdeh Formation was extended to more than 10 km in the southern and western sides of the Hengam diapir (Fig. 8), but was limited to the close proximity of the central Abu Musa and Greater Tonb diapirs (Figs. 6 and 7). Moreover, the geometry of the Gachsaran, Guri and Mishan depocentre axial traces (Figs. 6–8) suggest that the main flow direction of the Fars Salt was inwards around the Hengam diapir but outwards around the Abu Musa and Greater Tonb central diapirs. With these geometries interpreted in the seismic data, as well as cross-section restoration, we suggest there was a close relationship between the lateral extent of allochthonous salt bodies at the Palaeocene–Eocene level and the flow direction of the Fars Salt based on the fluid mechanics concept (i.e. pressure and elevation head gradients) (Fig. 16).

The degree of differential loading on the allochthonous Hormuz Salt emplaced during Palaeocene–Eocene times was likely depended upon its lateral extent, which consequently determined the dominant flow direction of the overlying Fars Salt (Fig. 16). The larger allochthonous salt sheet (more than ~10-km-long) in Hengam area could have allowed an efficient evacuation of the salt sheet in the frontal part, resulting in a tertiary weld that propagated towards the preexisting diapir. This modified the geometry of the Fars Salt layer and exerted a differential pressure which efficiently drove the lateral expulsion of the Fars Salt towards the preexisting diapir (i.e. inwards flow) because of the co-directional gradients in pressure head imposed by overburden thickness and elevation head imposed by top Fars Salt dip direction

(Fig. 16a2–4). Similar simplified relationships have been discussed by Rowan (2019) where the competition between the overburden thickness and density versus top-salt dip direction determines the direction of the salt flow. The progressive evacuation of the Fars Salt and the underlying sheet of Hormuz Salt in the Hengam area led to the formation of salt-evacuation minibasins above the Fars Salt and depocentre migration towards the preexisting diapir (Figs. 8 and 16a4). We suggest that gravitational loading was accommodated by both the Fars Salt and the underlying salt sheet (Fig. 16a4), which may account for the incomplete welding of the Fars Salt around the Hengam diapir (Fig. 8) compared to the Abu Musa and Greater Tonb (Figs. 6 and 7).

In the Abu Musa and Greater Tonb, the laterally smaller body (less than ~3-km-long) of the allochthonous Hormuz salt emplaced at Palaeocene–Eocene level (Figs. 6 and 7) accommodated a limited differential load (Fig. 16b2). Yet, this differential load appears to have sufficiently modified the geometry of the Fars Salt and imposed gradients of pressure and elevation head on it near the preexisting Hormuz-Salt diapir. The Fars Salt initially flowed in both directions and was evacuated to nucleate a primary weld near the central diapir (Fig. 16b3). It was followed by the change in the overlying depocentre position towards the areas of available Fars Salt along the flank of the isolated salt anticlines further away from the central diapir. The inflated pressurised salt lifted the roof of the inner salt anticline and exposed it to erosion. The roof thinned by erosion was, therefore, weak enough to trigger active diapirism and conversion of the salt anticline into a passive salt wall fed by thick Fars Salt from both sides (Fig. 16b3–4). Another salt anticline formed at the external part did not evolve into a salt wall because of the preferential flow of the salt into the adjacent passive wall. The passive salt wall was subsequently buried by younger sediments as the source layer was welded around it.

The inward-dipping extensional faults detached in the Fars Salt along the salt anticlines of Abu Musa and Greater Tonb (Figs. 6 and 7), or in the Hormuz-Salt sheet in the Hengam area (Fig. 8) suggest a component of gravitational failure of the Fars-Salt overburden. This overburden failure in the Hengam area was a response to tilting of the sedimentary succession overlying the Hengam salt sheet after it started evacuating back towards the central diapir. The gravitational failure of the overburden was also enhanced by the dipping Fars Salt towards the central diapir. In contrast, in the Greater Tonb and Abu Musa areas (Figs. 6 and 7), the expulsion of Fars Salt beneath the internal flank of the outer salt anticline led to flank collapse and gravitational failure of the roof regardless of a horizontal base of the Fars-Salt and the absence of a Hormuz-Salt sheet underlying it (Figs. 9k,l and 16b4–5).

A decrease in sedimentation rate relative to the salt-rise rate, lateral contraction, and development of expulsion rollover structures on the hangingwall side of a leaning diapir have been introduced as the drivers for increasing upward salt-rise rate and the development of allochthonous salt (Rowan, 2017). The relatively thick arched roof of the Fars-Salt walls (Figs. 6 and 7) indicate that they were rejuvenated by the Neogene contractional deformation of Zagros even though the source layer was already depleted (Fig. 9k,l) (see also Hassanpour et al., 2020; Snidero et al., 2020). This is also supported by the physical Model 2, where the extrusion of the upper polymer through the annular salt wall continued until the end of the experiment even though the source layer was welded out to the base of the polymer (Figs. 11 and 13). Furthermore, Fars-Salt evacuation and welding resulted in depocentre migration towards the salt wall flanks and subsided into the available salt. This process increased the salt supply into the diapir (Figs. 9 and 16), similar to what happens with the development of expulsion rollover structures (Rowan, 2017). Therefore, the development of shifting depocentres sinking into the Fars-Salt diapiric pedestals together with contractional squeezing of the diapirs by Zagros shortening increased the salt supply rate into the isolated salt walls and the central diapirs in the Hengam, Greater Tonb, and Abu Musa. The consequence was the diapir flaring, formation of salt wings in the Miocene intervals, as well as salt extrusion in the present-day islands (Figs. 6–8).

5.3. Kinematic interaction of the Hormuz and Fars salts

According to the interpretation of seismic data from the Eastern Persian Gulf, the Fars Salt has flowed and formed salt structures wherever preexisting Hormuz-Salt structures are in form of salt diapirs developing an allochthonous salt body prior to the deposition of the Fars Salt (Hengam, Greater Tonb, and Abu Musa diapirs), or deep-seated salt pillows (Tusan, Taftan, and Dustku pillows) (Figs. 5–8). In contrast, the Fars Salt does not show any evidence of lateral flow and salt structures around those diapirs of Hormuz Salt that lack salt sheets or wings underlying the Fars Salt (i.e. Lesser Tonb and Namakdan salt stocks in Fig. 5). Similarly, in the physical models (Figs. 10 and 11), the upper polymer (Fars Salt) remained static where no differential loading was imposed on it (Model 1), whereas flowed to form isolated salt structures where it was subjected to differential sedimentary loading around the Hormuz-Salt polymer stock (Model 2). In addition, cross-sections and depth slices show that the polymer layers and the salt structures had different histories concerning the kinematics of flow and diapirism. First, the stock was squeezed in both models and extruded polymer above the sand, but the amount of extruded polymer is considerably greater in Model 2 (Fig. 15c) than in Model 1 (Fig. 14c) despite the smaller amount of total shortening in Model 2 (57.2 mm) relative to Model 1 (72 mm). In Model 2, the diapiric annular wall sourced entirely by the upper polymer was also squeezed and extruded a significant amount of the upper polymer (Fig. 13). Second, the upper polymer flowed to form an isolated salt structure (annular wall) in the model where differential sedimentary loading was imposed (Model 2). Third, in Model 2, most of the upper polymer flowed into the annular wall rather than into the central stock (Fig. 13d,e), analogous to the proposed seismic interpretation of the Fars Salt in the Abu Musa and Greater Tonb areas (Figs. 6 and 7). The similarities and differences observed in the seismic data and physical models have several important implications as the following.

Initially, differential loading has triggered the Fars-Salt flow, whereas contractional deformation played an important role at later stages. In addition, to trigger salt flow, differential loading could have been produced by thickness variations (depositional or erosional) of the overburden (Gachsaran Fm.) similar to vacuuming off the sand in the models, or by the modification of the Fars Salt geometry due to evacuation of the underlying Hormuz Salt, or both. From the seismic data and cross-section restoration (Figs. 6–9), the sharp erosional truncation of the Gachsaran Formation adjacent to the Fars-Salt walls suggest that this formation initially formed the roof of the inflated Fars Salt. Subsequently, these strata were thinned and removed above the salt anticlines to allow their evolution into passive salt walls, meaning that overburden removal was slightly younger than the initial lateral flow of the Fars Salt (Fig. 16). Therefore, the absence of Fars-Salt flow around the Namakdan and Lesser Tonb stocks (Fig. 5) suggest that the Hormuz Salt was more likely mostly welded before the Fars Salt began flowing at Early Miocene. Primary welding of the autochthonous Hormuz Salt restricted the accommodation of differential loading, hence there was no differential pressure on the Fars Salt by overlying sediments. In contrast, evacuation of the salt sheets emplaced during Palaeocene-Eocene around the Hengam, Abu Musa, and Greater Tonb central diapirs could have favoured the accommodation of a differential sedimentary load on top of the Fars Salt, even if the autochthonous Hormuz Salt was already welded out.

In the studied area, the boundary between the Fars and Hormuz salts along the Abu Musa, Greater Tonb, and Hengam diapirs is not imaged in the seismic profiles. The physical models have the advantage of using different polymers having the same physical properties (i.e. density and viscosity; Table 2) but different colours, allowing us to track their spatial flow individually. In both models, the upper (green) polymer simulating the Fars Salt flowed and rose along the margin of the salt stock that is primarily fed by the lower (blue) polymer simulating the Hormuz Salt (Figs. 12 and 13). The model cross-sections show that the two polymers were not mixed even after their lateral extrusion. This point created us with the temptation to speculate that the Fars Salt is not mixed with the Hormuz Salt in the central Abu Musa, Greater Tonb, and Hengam diapirs, but rather forms a rim around the Hormuz Salt (Figs. 6–8 and 16). In addition, some of the upper polymer flanking the stock in Model 1 originated from its initial position at the roof of the lower polymer stock; shortening squeezed the stock upwards to actively arch and break through its roof, shouldering aside its overburden including the upper polymer. This also happened in Model 2, but there was additional inwards flow of the upper polymer due to the subsidence of minibasins expelling some of the polymer towards the central stock. These annular minibasins surrounding the central stock and the annular wall are welded out to the base of the upper polymer, and lateral thickness variation of sand layers within these minibasins suggest lateral migration of depocentres due to progressive salt evacuation and welding (Fig. 13), comparable to those interpreted above the Fars Salt around the Abu Musa, Greater Tonb, and Hengam salt structures (Figs. 6–9). These processes controlled the quantity of upper polymer rise and extrusion around the central stock margin despite the lower amount of total shortening in Model 2 than Model 1. The amount of influx of the upper polymer probably explains the development of salt wings in the Miocene intervals around the Hengam diapir (Fig. 8) but not around the central Abu Musa diapir (Fig. 6). The majority of Fars Salt flowed away from the central Abu Musa stock; conversely, the Fars Salt flowed essentially towards the Hengam stock, resulting in an increase of the salt inflation and extrusion in Miocene times when there was the greatest evacuation of the Fars Salt during the sedimentation of the Middle–Late Miocene Guri and Mishan intervals.

5.4. Some comparisons with other salt basins containing multiple mobile salt layers

The kinematic linkage of the Fars-Salt flow and diapirism to the presence of allochthonous Hormuz Salt extruded from diapirs, and the development of annular salt walls and minibasins related to the younger salt layer is a unique phenomenon in the Eastern Persian Gulf among the salt basins. Although multiple evaporitic layers are known in many salt basins, multiple mobile salt layers have been recently recognised – in addition to the Eastern Persian Gulf – in the Danmarkshavn Ridge and adjacent basins of Northeast Greenland shelf associated with the presence of at least two, and possibly four, distinct mobile levels of Pennsylvanian to Early Permian age (Rowan and Jarvie, 2020), and in the Slyne and Erris basins of offshore Northwest Ireland involving the Zechstein (Upper Permian) and the Uilleann (Upper Triassic) mobile salt layers (Corcoran and Mecklenburgh, 2005; O'Sullivan et al., 2021). Yet, there are large differences between the salt-related structural styles in the Eastern Persian Gulf and these basins along the North Atlantic margins. First, the autochthonous Hormuz and Fars salts in the Eastern Persian Gulf are separated by a thick (~9–12 km) sedimentary interval if our interpreted top Hormuz Salt reflector is in the correct position and the depth conversion is valid. In contrast, the mobile salt layers are separated by a thinner sedimentary interval (~4–8 km thick) in the Northeast Greenland shelf (Rowan and Jarvie, 2020, their Fig. 7) and by a Lower Triassic interval with a thickness of only ~170–200 ms TWT (O'Sullivan et al., 2021) corresponding to ~330–400 m in offshore Northwest Ireland (Dancer et al., 2005; C. O'Sullivan, pers. comm., 2021). However, these comparatively thinner sedimentary sections between the mobile salt layers in the North Atlantic margin basins are relatively more comparable in thickness to the sedimentary interval separating the Fars Salt from the allochthonous Hormuz Salt emplaced at Palaeocene–Eocene and Miocene times in the Eastern Persian Gulf. Second, both lower (Hormuz) and upper (Fars) salt levels in the Eastern Persian Gulf have formed large salt walls and stocks. In contrast, the shallow salt in the Northeast Greenland shelf is associated with diapirs but the deeper salt is only a detachment surface within which extensional faults sole out (Rowan and Jarvie, 2020), and apparently there in no specific spatial linkage between the development of the structures related to both salts. Similarly, O'Sullivan et al. (2021) interpreted gentle salt rollers and pillows in the lower (Upper Permian) salt overlain by salt rollers and in one case a gentle salt wall of the upper salt (Upper Triassic) that are stratigraphically discrete but kinematically linked. In other words, the Triassic salt has formed salt structures only where there is a salt structure in the deeper salt, and thus is to some extent comparable to the kinematic linkage of the Fars and Hormuz Salt in the Eastern Persian Gulf.

6. Conclusions

A distinctive salt-tectonic structural style stands out in the Eastern Persian Gulf due to overlapping of two autochthonous salt layers, which are the Ediacaran–Early Cambrian Hormuz Salt and the Oligocene–Early Miocene Fars Salt. The Hormuz Salt is present regionally and formed several salt walls and stocks, as well as salt pillows. Development of these structures began at Cambrian(?) times once the sediments loaded the salt layer, and the resultant diapirs rose passively during Palaeozoic and Mesozoic times and were rejuvenated by episodic contractional deformation events in Cenozoic. The Fars Salt was deposited in a local basin, and its flow led to the formation of several salt walls and anticlines around the preexisting diapirs of Hormuz Salt, or gentle salt pillows above the deeply buried pillows of the Hormuz Salt. In addition, allochthonous sheets and wings of the Hormuz Salt were extruded from some diapirs and emplaced at Palaeocene–Eocene and Early–Middle Miocene before and after the deposition of the Fars Salt, respectively, which further puzzled the geometric relationships between these two salt layers and their structures in the seismic data.

Seismic profiles interpretation calibrated by exploration well data indicated that the Fars Salt was evacuated and formed salt structures wherever it interacted with those diapirs of the Hormuz Salt that extruded allochthonous salt sheets or wings prior to the Fars Salt deposition (i.e. in the Hengam, Greater Tonb, and Abu Musa areas). In contrast, Fars-Salt structures did not form around those diapirs of Hormuz Salt that lack allochthonous salt at Palaeocene–Eocene levels (i.e. Namakdan and Lesser Tonb stocks). In addition, the allochthonous bodies of the Hormuz Salt at Palaeocene–Eocene level had different lateral extents from the edges of their salt feeders. The interpreted seismic profiles and results of sequential cross-section restoration illustrate that the Fars Salt was more likely triggered by loading of these salt sheets and wings underlying the Fars Salt as the evacuation or rearrangement of the salt within these sheets / wings modified the geometry of the Fars Salt and triggered its lateral flow. The driving force was most probably differential sedimentary loading that led to gradients of pressure and elevation head on top of the Fars Salt. The onset of the Fars Salt evacuation–inflation was coeval with contractional deformation in the Oman–Zagros orogenic belts. The role of layer-parallel shortening in contribution to the flow initiation, therefore, cannot be ruled out although the interpreted seismic data and physical modelling results suggest that differential sedimentary loading had the primary role in triggering the initial flow at the early stages of salt evacuation and rise, and lateral contraction was more influential at later stages by squeezing the salt structures mainly since Late Miocene. Following the initial flow, the subsequent kinematics of the Fars-Salt flow was controlled by the degree of evacuation of the underlying salt bodies that, in turn, was dependent upon their lateral extents. The larger salt sheet at Hengam was efficiently evacuated back towards the preexisting diapir, hence controlled the Fars-Salt flow direction and evacuation to the same direction (i.e. towards the preexisting diapir). Conversely, the smaller pre-Fars salt sheets / wings at Abu Musa and Greater Tonb allowed limited evacuation, and the resulting differential load on the Fars Salt started its flow near the preexisting diapirs, leading to primary welding. The availability of the Fars Salt at farther areas drove the migration of depocentres away from the preexisting diapir, reversing the Fars-Salt dominant flow direction. It led to the development of salt walls and anticlines around the preexisting diapirs. These salt-evacuation mini-basins contain stacked shifting depocentres above the welded Fars Salt.

Credit author statement

Jafar Hassanpour: Conceptualisation; Data curation; Formal analysis; Investigation; Methodology; Validation; Visualisation; Writing - original draft; Writing - review & editing. **Josep Anton Muñoz:** Supervision; Conceptualisation; Methodology; Validation; Visualisation; Writing - original draft; Writing - review & editing; Funding acquisition. **Ali Yassaghi:** Supervision; Conceptualisation; Data curation; Validation; Visualisation; Writing - original draft; Writing - review & editing. **Oriol Ferrer:** Conceptualisation; Methodology; Validation; Visualisation; Writing - original draft; Writing - review & editing. **Salman Jahani:** Investigation; Visualisation; Writing - review & editing. **Pablo Santolaria:** Conceptualisation; Methodology; Validation; Visualisation; Writing - original draft; Writing - review & editing. **Seyed Mohsen SeyedAli:** Data curation; Visualisation; Writing - review & editing.

Declaration of Competing Interest

The authors declare that they have no known competing financial interests or personal relationships that could have appeared to influence the work reported in this paper.

Acknowledgements

We are grateful to the Iranian Offshore Oil Company (IOOC) for providing seismic data and permission to publish this paper. Jafar Hassanpour appreciates Institut de Recerca Geomodels of the Universitat de Barcelona for providing the opportunity to use the Geomodels Analog Modelling Laboratory, a Scientific Infrastructure (UNBA08-4E-006) provided by the European Regional Development Fund of the Ministerio de Ciencia e Innovación of the Spanish Government and Equinor (former Statoil). He also acknowledges financial support by Tarbiat Modares University (Iran) during his stay in Barcelona. Physical modelling work was supported by the project SALCONBELT (CGL2017-85532-P) funded by AEI/FEDER, UE (Agencia Estatal de Investigación/Fondo Europeo de Desarollo Regional) of the Ministerio de Economía y Competitividad. Núria Carrera helped with the modelling setup at the Institut de Recerca Geomodels, and Farhad Nafisi helped to convert the physicsl model sections into pseudo-seismic volume. Petroleum Experts (PETEX) is acknowledged for providing Move software for cross-section restoration. We thank two anonymous reviewers for providing insightful comments that led to further improvement of the paper, and Associate Editor Ramon Carbonell for editorial handling.

References

Agard, P., Omrani, J., Jolivet, L., Whitechurch, H., Vrielynck, B., Spakman, W., Monié, P., Meyer, B., Wortel, R., 2011. Zagros orogeny: a subduction-dominated process. In: Lacombe, O., Grasemann, B., Simpson, G. (Eds.), Geodynamic Evolution of the Zagros, Geological Magazine, 148, pp. 692–725. https://doi.org/10.1017/S001675681100046X, 5–6.
Alavi, M., 2004. Regional stratigraphy of the Zagros fold-thrust belt of Iran and its proforeland evolution. Am. J. Sci. 304, 1–20. https://doi.org/10.2475/ajs.304.1.1.
Albertz, M., Beaumont, C., Shimeld, J.W., Ings, S.J., Gradmann, S., 2010. An investigation of salt tectonic structural styles in the Scotian Basin offshore Atlantic Canada: 1. Comparison of observations with geometrically simple numerical models. Tectonics 29 (4). https://doi.org/10.1029/2009TC002539. TC4017.
Al-Husseini, M.I., 2000. Origin of the Arabian Plate structures: Amar collision and Najd rift. GeoArabia 5 (4), 527–542.
Al-Husseini, M.I., 2014. Ediacaran–Cambrian Middle East Geologic Time Scale 2014: Proposed correlation of Oman's Abu Mahara Supergroup and Saudi Arabia's Jibalah Group. GeoArabia 19 (2), 107–132.
Al-Husseini, M.I., 2015. Arabian Orbital Stratigraphy revisited – AROS 2015. GeoArabia 20 (4), 183–216.
Ali, M.Y., Watts, A.B., 2009. Subsidence history, gravity anomalies and flexure of the United Arab Emirates (UAE) foreland basin. GeoArabia 14 (2), 17–44.
Allen, P.A., 2007. The Huqf Supergroup of Oman: Basin development and context for Neoproterozoic glaciation. Earth Sci. Rev. 84 (3), 139–185. https://doi.org/10.1016/j.earscirev.2007.06.005.
Athy, L.F., 1930. Density, porosity, and compaction of sedimentary rocks. AAPG Bull. 14 (1), 1–24. https://doi.org/10.1306/3D93289E-16B1-11D7-8645000102C1865D.
Berberian, M., 1995. Master "blind" thrust faults hidden under the Zagros folds: active basement tectonics and surface morphotectonics. Tectonophysics 241 (3), 193–224. https://doi.org/10.1016/0040-1951(94)00185-C.
Berberian, M., King, G.C.P., 1981. Towards a paleogeography and tectonic evolution of Iran. Can. J. Earth Sci. 18 (2), 210–265. https://doi.org/10.1139/e81-019.
Berra, F., Carminati, E., 2010. Subsidence history from a backstripping analysis of the Permo-Mesozoic succession of the Central Southern Alps (Northern Italy). Basin Res. 22, 952–975. https://doi.org/10.1111/j.1365-2117.2009.00453.x.
Bonini, M., 2003. Detachment folding, fold amplification, and diapirism in thrust wedge experiments. Tectonics 22 (6), 1065. https://doi.org/10.1029/2002TC001458.
Boote, D.R.D., Mou, D., Waite, R.I., 1990. Structural evolution of the Suneinah foreland, Central Oman Mountains. In: Robertson, A.H.F., Searle, M.P., Ries, A.C. (Eds.), The Geology and Tectonics of the Oman Region, Geological Society, London, Special Publications, 49, pp. 397–418. https://doi.org/10.1144/GSL.SP.1992.049.01.25, 1.
Bosák, P., Jaroš, J., Spudil, J., Sulovský, P., Václavek, V., 1998. Salt Plugs in the Eastern Zagros, Iran: Results of Regional Geological Reconnaissance. Geolines, Praha: GlÚ AV ČR Praha, 7, 3–180. Geological Institute, Academy of Sciences of the Czech Republic.
Bowring, S.A., Grotzinger, J.P., Condon, D.J., Ramezani, J., Newall, M.J., Allen, P.A., 2007. Geochronologic constraints on the chronostratigraphic framework of the Neoproterozoic Huqf Supergroup, Sultanate of Oman. Am. J. Sci. 307 (10), 1097–1145. https://doi.org/10.2475/10.2007.01.
Brun, J.-P., Fort, X., 2011. Salt tectonics at passive margins: Geology versus models. Mar. Pet. Geol. 28, 1123–1145. https://doi.org/10.1016/j.marpetgeo.2011.03.004.
Burberry, C.M., 2015. Spatial and temporal variation in penetrative strain during compression: Insights from analog models. Lithosphere 7 (6), 611–624. https://doi.org/10.1130/L454.1.
Callot, J.-P., Jahani, S., Letouzey, J., 2007. The role of pre-existing diapirs in fold and thrust belt development. In: Lacombe, O., Lavè, J., Roure, F., Vergès, J. (Eds.), Thrust Belts and Foreland Basins. Springer, Berlin, pp. 309–325. https://doi.org/10.1007/978-3-540-69426-7_16.
Callot, J.-P., Trocmé, V., Letouzey, J., Albouy, E., Jahani, S., Sherkati, S., 2012. Pre-existing salt structures and the folding of the Zagros Mountains. In: Alsop, G.I., Archer, S.G., Hartley, A.J., Grant, N.T., Hodgkinson, R. (Eds.), Salt Tectonics, Sediments and Prospectivity, Geological Society, London, Special Publications, 363, pp. 545–561. https://doi.org/10.1144/SP363.27.
Corcoran, D.V., Mecklenburgh, R., 2005. Exhumation of the Corrib Gas Field, Slyne Basin, offshore Ireland. Pet. Geosci. 11 (3), 239–256. https://doi.org/10.1144/1354-079304-637.
Corradetti, A., Spina, V., Tavani, S., Ringenbach, J.-C., Sabbatino, M., Razin, P., Laurent, O., Brichau, S., Mazzoli, S., 2020. Late-stage tectonic evolution of the Al-Hajar Mountains, Oman: new constraints from Palaeogene sedimentary units and low-temperature thermochronometry. Geol. Mag. 157, 1031–1044. https://doi.org/10.1017/S0016756819001250.
Dancer, P.N., Kenyon-Roberts, S.M., Downey, J.W., Baillie, J.M., Meadows, N.S., Maguire, K., 2005. The Corrib gas field, offshore west of Ireland. Petroleum Geology: North-West Europe and Global Perspectives. Geol. Soc. London 6, 1035–1046. https://doi.org/10.1144/0061035.
Davison, I., Alsop, I., Birch, P., Elders, C., Evans, N.G., Nicholson, H., Rorison, P., Wade, D., Woodward, J., Young, M., 2000. Geometry and late-stage structural evolution of Central Graben salt diapirs, North Sea. Mar. Pet. Geol. 17 (4), 499–522. https://doi.org/10.1016/S0264-8172(99)00068-9.
Del Ventisette, C., Montanari, D., Bonini, M., Sani, F., 2005. Positive fault inversion triggering 'intrusive diapirism': an analogue modelling perspective. Terra Nova 17, 478–485. https://doi.org/10.1111/j.1365-3121.2005.00637.x.
Dell'Ertole, D., Schellart, W.P., 2013. The development of sheath folds in viscously stratified materials in simple shear conditions: an analogue approach. J. Struct. Geol. 56, 129–141. https://doi.org/10.1016/j.jsg.2013.09.002.
Dooley, T.P., Jackson, M.P.A., Hudec, M.R., 2009a. Inflation and deflation of deeply buried salt stocks during lateral shortening. J. Struct. Geol. 31, 582–600. https://doi.org/10.1016/j.jsg.2009.03.013.
Dooley, T.P., Jackson, M.P.A., Hudec, M.R., 2009b. Deformation styles and linkage of salt walls during oblique shortening. AAPG Annual Convention 18, 57.
Dooley, T.P., Hudec, M.R., Jackson, M.P.A., 2012. The structure and evolution of sutures in allochthonous salt. AAPG Bull. 96 (6), 1045–1070. https://doi.org/10.1306/09231111036.
Dooley, T.P., Jackson, M.P.A., Hudec, M.R., 2015. Breakout of squeezed stocks: dispersal of roof fragments, source of extrusive salt and interaction with regional thrust faults. Basin Res. 27 (1), 3–25. https://doi.org/10.1111/bre.12043.
Droste, H.J., 1997. Stratigraphy of the lower Paleozoic Haima Supergroup of Oman. GeoArabia 2 (4), 419–472.
Duffy, O.B., Dooley, T.P., Hudec, M.R., Jackson, M.P.A., Fernandez, N., Jackson, C.A.-L., Soto, J.I., 2018. Structural evolution of salt-influenced fold-and-thrust belts: a synthesis and new insights from basins containing isolated salt diapirs. J. Struct. Geol. 114, 206–221. https://doi.org/10.1016/j.jsg.2018.06.024.
Edgell, H.S., 1996. Salt tectonism in the Persian Gulf Basin. In: Alsop, G.I., Blundell, D.J., Davison, I. (Eds.), Salt Tectonics, Geological Society, London, Special Publications, 100, pp. 129–151. https://doi.org/10.1144/GSL.SP.1996.100.01.10.
Ezati Asl, M., Faghih, A., Mukherjee, S., Soleimany, B., 2019. Style and timing of salt movement in the Persian Gulf basin, offshore Iran: Insights from halokinetic

sequences adjacent to the Tonb-e-Bozorg salt diapir. J. Struct. Geol. 122, 116–132. https://doi.org/10.1016/j.jsg.2019.02.002.
Faghih, A., Ezati Asl, M., Mukherjee, S., Soleimany, B., 2019. Characterizing halokinesis and timing of salt movement in the Abu Musa salt diapir, Persian Gulf, offshore Iran. Mar. Pet. Geol. 105, 338–352. https://doi.org/10.1016/j.marpetgeo.2019.04.002.
Faqira, M., Rademakers, M., Afifi, A.M., 2009. New insights into the Hercynian Orogeny, and their implications for the Paleozoic Hydrocarbon System in the Arabian Plate. GeoArabia 14 (3), 199–228.
Faramarzi, N.S., Amini, S., Schmitt, A.K., Hassanzadeh, J., Borg, G., McKeegan, K., Razavi, S.M.H., Mortazavi, S.M., 2015. Geochronology and geochemistry of rhyolites from Hormuz Island, southern Iran: a new record of Cadomian arc magmatism in the Hormuz Formation. Lithos 236, 203–211. https://doi.org/10.1016/j.lithos.2015.08.017.
Ferrer, O., McClay, K.R., Sellier, N.C., 2016. Influence of fault geometries and mechanical anisotropies on the growth and inversion of hanging-wall synclinal basins: insights from sandbox models and natural examples. In: Childs, C.J., Holdsworth, R.E., Jackson, C.A.-L., Manzocchi, T., Walsh, J.J., Yielding, G. (Eds.), The Geometry and Growth of Normal Faults, Geological Society, London, Special Publications, 439, pp. 487–509. https://doi.org/10.1144/SP439.8.
Ferrer, O., Roca, E., Gratacós, O., Muñoz, J.A., 2017. Modeling the interaction between presalt seamounts and gravitational failure in salt-bearing passive margins: the Messinian case in the northwestern Mediterranean Basin. Interpretation 5 (1), SD99–SD117. https://doi.org/10.1190/INT-2016-0096.1.
Frizon de Lamotte, D., Raulin, C., Mouchot, N., Wrobel-Daveau, J.-C., Blanpied, C., Ringenbach, J.-C., 2011. The southernmost margin of the Tethys realm during the Mesozoic and Cenozoic: initial geometry and timing of the inversion processes. Tectonics 30 (3), TC3002. https://doi.org/10.1029/2010TC002691.
Gardner, G.H.F., Gardner, L.W., Gregory, A.R., 1974. Formation velocity and density – the diagnostic basics for stratigraphic traps. Geophysics 39 (6), 770–780. https://doi.org/10.1190/1.1440465.
Ge, H., Jackson, M.P.A., Vendeville, B.C., 1997. Kinematics and dynamics of salt tectonics driven by progradation. AAPG Bull. 81 (3), 398–423.
Gemmer, L., Ings, S.J., Medvedev, S., Beaumont, C., 2004. Salt tectonics driven by differential sediment loading: stability analysis and finite-element experiments. Basin Res. 16, 199–218. https://doi.org/10.1111/j.1365-2117.2004.00229.x.
Giles, K.A., Lawton, T.F., 2002. Halokinetic sequence stratigraphy adjacent to the El Papalote diapir, northeastern Mexico. AAPG Bull. 86 (5), 823–840. https://doi.org/10.1306/61EEDBAC-173E-11D7-8645000102C1865D.
Glennie, K.W., Boeuf, M.G.A., Hughes Clarke, M.W., Moody-Stuart, M., Pilaar, W., Reinhardt, B.M., 1974. Geology of the Oman Mountains. Verhandelingen van het Koninglijk Nederlands Geologisch Mijnbouwkundig Genootschap, 31, 423 p.
Hammerstein, J.A., Truelove, L., McClay, K.R., 2014. Additional methods for the analysis of seismic data and risk reduction through the interpretation and reservoir modelling of scaled analogue models. AAPG Search Discov. Article #90189.
Hansman, R.J., Ring, U., Thomson, S.N., den Brok, B., Stübner, K., 2017. Late Eocene uplift of the Al Hajar Mountains, Oman, supported by stratigraphy and low-temperature thermochronology. Tectonics 36 (12), 3081–3109. https://doi.org/10.1002/2017TC004672.
Hassanpour, J., Jahani, S., Ghassemi, M.R., Alavi, S.A., Zeinali, F., 2018. Evolution of the Karebas Fault System and adjacent folds, central Zagros fold-and-thrust belt, Iran: Role of pre-existing halokinesis (salt structures and minibasins) and detachment levels. J. Asian Earth Sci. 164, 125–142. https://doi.org/10.1016/j.jseaes.2018.06.024.
Hassanpour, J., Yassaghi, A., Muñoz, J.A., Jahani, S., 2020. Salt tectonics in a double salt-source layer setting (Eastern Persian Gulf, Iran): Insights from interpretation of seismic profiles and sequential cross-section restoration. Basin Res. 33, 159–185. https://doi.org/10.1111/bre.12459.
Hessami, K., Koyi, H.A., Talbot, C.J., Tabasi, H., Shabanian, E., 2001. Progressive unconformities within an evolving foreland fold–thrust belt, Zagros Mountains. J. Geol. Soc. Lond. 158 (6), 969–981. https://doi.org/10.1144/0016-764901-007.
Horsfield, W.T., 1977. An experimental approach to basement-controlled faulting. Geol. Mijnb. 56, 363–370.
Hubbert, M.K., 1951. Mechanical basis for certain familiar geologic structures. Geol. Soc. Am. Bull. 62 (4), 355–372. https://doi.org/10.1130/0016-7606(1951)62[355:MBFCFG]2.0.CO;2.
Hudec, M.R., Jackson, M.P.A., 2007. Terra infirma: Understanding salt tectonics. Earth Sci. Rev. 82 (1), 1–28. https://doi.org/10.1016/j.earscirev.2007.01.001.
Jackson, M.P.A., Hudec, M.R., 2017. Salt Tectonics: Principles and Practice. Cambridge University Press, First ed, p. 498.
Jackson, M.P.A., Vendeville, B.C., 1994. Regional extension as a geologic trigger for diapirism. Geol. Soc. Am. Bull. 106, 57–73 doi:10.1130/0016-7606 (1994) 106<0057:REAAGT>2.3.CO;2.
Jahani, S., Callot, J.-P., Frizon de Lamotte, D., Letouzey, J., Leturmy, P., 2007. The salt diapirs of the eastern Fars province (Zagros, Iran): A brief outline of their past and present. In: Lacombe, O., Lavè, J., Roure, F., Vergès, J. (Eds.), Thrust Belts and Foreland Basins. Springer, Berlin, pp. 289–308. https://doi.org/10.1007/978-3-540-69426-7_15.
Jahani, S., Callot, J.-P., Letouzey, J., Frizon de Lamotte, D., 2009. The eastern termination of the Zagros Fold-and-Thrust Belt, Iran: Structures, evolution, and relationships between salt plugs, folding, and faulting. Tectonics 28 (6), TC6004. https://doi.org/10.1029/2008TC002418.
Jahani, S., Hassanpour, J., Mohammadi-Firouz, S., Letouzey, J., Frizon de Lamotte, D., Alavi, S.A., Soleimany, B., 2017. Salt tectonics and tear faulting in the central part of the Zagros Fold-Thrust Belt, Iran. Mar. Pet. Geol. 86, 426–446. https://doi.org/10.1016/j.marpetgeo.2017.06.003.
James, G.A., Wynd, J.G., 1965. Stratigraphic nomenclature of Iranian oil consortium agreement area. AAPG Bull. 49 (12), 2182–2245.
Kent, P.E., 1979. The emergent Hormuz salt plugs of southern Iran. J. Pet. Geol. 2 (2), 117–144. https://doi.org/10.1111/j.1747-5457.1979.tb00698.x.
Khadivi, S., Mouthereau, F., Larrasoaña, J.C., Vergés, J., Lacombe, O., Khademi, E., Beamud, E., Melinte-Dobrinescu, M., Suc, J.P., 2010. Magnetochronology of synorogenic Miocene foreland sediments in the Fars arc of the Zagros Folded Belt (SW Iran). Basin Res. 22 (6), 918–932. https://doi.org/10.1111/j.1365-2117.2009.00446.x.
Khadivi, S., Mouthereau, F., Barbarand, J., Adatte, T., Lacombe, O., 2012. Constraints on palaeodrainage evolution induced by uplift and exhumation on the southern flank of the Zagros–Iranian Plateau. J. Geol. Soc. Lond. 169, 83–97. https://doi.org/10.1144/0016-76492011-031.
Koyi, H.A., Sans, M., Teixell, A., Cotton, J.T., Zeyen, H., 2004. The significance of penetrative strain in the restoration of shortened layers – Insights from sand models and the Spanish Pyrenees. In: McClay, K.R. (Ed.), Thrust Tectonics and Hydrocarbon Systems, AAPG Memoir, 82, pp. 1–16. https://doi.org/10.1306/M82813C11.
Krantz, R.W., 1991. Measurements of friction coefficients and cohesion for faulting and fault reactivation in laboratory models using sand and sand mixtures. Tectonophysics 188, 203–207. https://doi.org/10.1016/0040-1951(91)90323-K.
Lashgari, A., Heyhat, M.R., Vergés, J., Beamud, E., Najafi, M., Khatib, M.M., Karimnejad, H.R., 2020. Age of synorogenic deposits and timing of folding in Dezful embayment, SW Zagros Fold Belt. Mar. Pet. Geol. 113, 104–148. https://doi.org/10.1016/j.marpetgeo.2019.104148.
Letouzey, J., Sherkati, S., 2004. Salt movement, tectonic events, and structural style in the central Zagros fold and thrust belt (Iran). In: 24th Annual GCSSEPM Foundation Bob F. Perkins Research Conference: Salt-Sediment Interactions and Hydrocarbon Prospectivity: Concepts, applications, and Case Studies for the 21st Century, Gulf Coast Section. SEPM, Houston, Texas.
Letouzey, J., Colletta, B., Vially, R., Chermette, J.C., 1995. Evolution of salt-related structures in compressional settings. In: Jackson, M.P.A., Roberts, D.G., Snelson, S. (Eds.), Salt Tectonics: A Global Perspective, AAPG Memoir, vol. 65, pp. 41–60.
Li, S., Abe, S., Reuning, L., Becker, S., Urai, J.L., Kukla, P.A., 2012. Numerical modelling of the displacement and deformation of embedded rock bodies during salt tectonics: a case study from the South Oman Salt Basin. In: Alsop, G.I., Archer, S.G., Hartley, A. J., Grant, N.T., Hodgkinson, R. (Eds.), Salt Tectonics, Sediments and Prospectivity, Geological Society, London, Special Publications, 363, pp. 503–520. https://doi.org/10.1144/SP363.24.
Lohrmann, J., Kukowski, N., Adam, J., Oncken, O., 2003. The impact of analogue material properties on the geometry, kinematics, and dynamics of convergent sand wedges. J. Struct. Geol. 25, 1691–1711. https://doi.org/10.1016/S0191-8141(03)00005-1.
Miller, S.L.M., Stewart, R.R., 1991. The relationship between elastic-wave velocities and density in sedimentary rocks: a proposal. Crewes Res. Rep. 3, 260–273.
Mouthereau, F., Lacombe, O., Vergés, J., 2012. Building the Zagros collisional orogen: timing, strain distribution and the dynamics of Arabia/Eurasia plate convergence. Tectonophysics 532, 27–60. https://doi.org/10.1016/j.tecto.2012.01.022.
Mukherjee, S., Talbot, C.J., Koyi, H.A., 2010. Viscosity estimates of salt in the Hormuz and Namakdan salt diapirs, Persian Gulf. Geol. Mag. 147 (4), 497–507. https://doi.org/10.1017/S001675680999077X.
Najafi, M., Beamud, E., Ruh, J.B., Mouthereau, F., Tahmasbi, A., Bernaola, G., Yassaghi, A., Motamedi, H., Sherkati, S., Goodarzi, M.G.H., Vergés, J., 2020. Pliocene growth of the Dowlatabad syncline in Frontal Fars arc: Folding propagation across the Zagros Fold Belt, Iran. Geol. Soc. Am. Bull. https://doi.org/10.1130/B35748.1.
Nehlig, P., Genna, A., Asfirane, F., 2002. A review of the Pan-African evolution of the Arabian Shield. GeoArabia 7 (1), 103–124.
Nilsen, K.T., Vendeville, B.C., Johansen, J.T., 1995. Influence of regional tectonics on halokinesis in the Nordkapp Basin, Barents Sea. In: Jackson, M.P.A., Roberts, D.G., Snelson, S. (Eds.), Salt Tectonics: A Global Perspective, AAPG Memoir, vol. 65, pp. 413–436.
Orang, K., Motamedi, H., Azadikhah, A., Royatvand, M., 2018. Structural framework and tectono-stratigraphic evolution of the eastern Persian Gulf, offshore Iran. Mar. Pet. Geol. 91, 89–107. https://doi.org/10.1016/j.marpetgeo.2017.12.014.
O'Sullivan, C.M., Childs, C.J., Saqab, M.M., Walsh, J.J., Shannon, P.M., 2021. The influence of multiple salt layers on rift-basin development; the Slyne and Erris basins, offshore NW Ireland. Basin Res. https://doi.org/10.1111/bre.12546.
Perotti, C.R., Chiariotti, L., Bresciani, I., Cattaneo, L., Toscani, G., 2016. Evolution and timing of salt diapirism in the Iranian sector of the Persian Gulf. Tectonophysics 679, 180–198. https://doi.org/10.1016/j.tecto.2016.04.040.
Pichel, L.M., Finch, E., Husse, M., Redfern, J., 2017. The influence of shortening and sedimentation on rejuvenation of salt diapirs: a new Discrete-Element Modelling approach. J. Struct. Geol. 103, 61–79. https://doi.org/10.1016/j.jsg.2017.09.016.
Pirouz, M., Simpson, G., Chiaradia, M., 2015. Constraint on foreland basin migration in the Zagros mountain belt using Sr isotope stratigraphy. Basin Res. 27 (6), 714–728. https://doi.org/10.1111/bre.12097.
Pirouz, M., Avouac, J.-P., Hassanzadeh, J., Kirschvink, J.L., Bahroudi, A., 2017. Early Neogene foreland of the Zagros, implications for the initial closure of the Neo-Tethys and kinematics of crustal shortening. Earth Planet. Sci. Lett. 477, 168–182. https://doi.org/10.1016/j.epsl.2017.07.046.
Piryaei, A., Reijmer, J.J.G., Borgomano, J., van Buchem, F.S.P., 2011. Late Cretaceous tectonic and sedimentary evolution of the Bandar Abbas area, Fars region, southern Iran. J. Pet. Geol. 34 (2), 157–180. https://doi.org/10.1111/j.1747-5457.2011.00499.x.
Pla, O., Roca, E., Xie, H., Izquierdo-Llavall, E., Muñoz, J.A., Rowan, M.G., Ferrer, O., Gratacós, O., Yuan, N., Huang, S., 2019. Influence of syntectonic sedimentation and

décollement rheology on the geometry and evolution of orogenic wedges: Analog modeling of the Kuqa fold-and-thrust belt (NW China). Tectonics 38 (8), 2727–2755. https://doi.org/10.1029/2018TC005386.
Player, R.A., 1969. Salt diapirs study. In: National Iranian Oil Company, Exploration Division, Tehran, Report No. 1146 unpublished.
Rodriguez, C.R., Jackson, C.A.-L., Rotevatn, A., Bell, R.E., Francis, M., 2018. Dual tectonic-climatic controls on salt giant deposition in the Santos Basin, offshore Brazil. Geosphere 14 (1), 215–242. https://doi.org/10.1130/GES01434.1.
Roma, M., Ferrer, O., McClay, K.R., Muñoz, J.A., Roca, E., Gratacós, O., Cabello, P., 2018a. Weld kinematics of syn-rift salt during basement-involved extension and subsequent inversion: results from analog models. Geol. Acta 16 (4), 391–410. https://doi.org/10.1344/GeologicaActa2018.16.4.4.
Roma, M., Ferrer, O., Roca, E., Pla, O., Escosa, F.O., Butillé, M., 2018b. Formation and inversion of salt-detached ramp-syncline basins. Results from analog modeling and application to the Columbrets Basin (Western Mediterranean). Tectonophysics 745, 214–228. https://doi.org/10.1016/j.tecto.2018.08.012.
Rowan, M.G., 1993. A systematic technique for the sequential restoration of salt structures. Tectonophysics 228 (3–4), 331–348. https://doi.org/10.1016/0040-1951(93)90347-M.
Rowan, M.G., 2017. An overview of allochthonous salt tectonics. In: Soto, J.I., Flinch, J. F., Tari, G. (Eds.), Permo-Triassic Salt Provinces of Europe, North Africa and the Atlantic Margins. Elsevier, pp. 97–114. https://doi.org/10.1016/B978-0-12-809417-4.00005-7.
Rowan, M.G., 2019. Conundrums in loading-driven salt movement. J. Struct. Geol. 125, 256–261. https://doi.org/10.1016/j.jsg.2018.04.010.
Rowan, M.G., Giles, K.A., 2021. Passive versus active salt diapirism. AAPG Bull. 105 (1), 53–63.
Rowan, M.G., Jarvie, A., 2020. Crustal extension and salt tectonics of the Danmarkshavn Ridge and adjacent basins, NE Greenland. Mar. Pet. Geol. 117, 104339. https://doi.org/10.1016/j.marpetgeo.2020.104339.
Rowan, M.G., Ratliff, R.A., 2012. Cross-section restoration of salt-related deformation: best practices and potential pitfalls. J. Struct. Geol. 41, 24–37. https://doi.org/10.1016/j.jsg.2011.12.012.
Rowan, M.G., Vendeville, B.C., 2006. Foldbelts with early salt withdrawal and diapirism: physical model and examples from the northern Gulf of Mexico and the Flinders Ranges, Australia. Mar. Pet. Geol. 23 (9), 871–891. https://doi.org/10.1016/j.marpetgeo.2006.08.003.
Rowan, M.G., Lawton, T.F., Giles, K.A., Ratliff, R.A., 2003. Near-salt deformation in La Popa basin, Mexico, and the northern Gulf of Mexico: a general model for passive diapirism. AAPG Bull. 87 (5), 733–756. https://doi.org/10.1306/01150302012.
Rowan, M.G., Peel, F.J., Vendeville, B.C., 2004. Gravity-driven fold belts on passive margins. In: McClay, K.R. (Ed.), Thrust Tectonics and Hydrocarbon Systems, AAPG Memoir, 82, pp. 157–182. https://doi.org/10.1306/M82813C9.
Ruh, J.B., Hirt, A.M., Burg, J.P., Mohammadi, A., 2014. Forward propagation of the Zagros Simply Folded Belt constrained from magnetostratigraphy of growth strata. Tectonics 33, 1534–1551. https://doi.org/10.1002/2013TC003465.
Santolaria, P., Ferrer, O., Rowan, M.G., Snidero, M., Carrera, N., Granado, P., Muñoz, J. A., Roca, E., Schneider, C.L., Piña, A., Zamora, G., 2021. Influence of pre-existing salt diapirs during thrust wedge evolution and secondary welding: Insights from analog modeling. J. Struct. Geol. (in press).
Schmoker, J.W., Halley, R.B., 1982. Carbonate porosity versus depth: a predictable relation for South Florida. AAPG Bull. 66 (12), 2561–2570. https://doi.org/10.1306/03B5AC73-16D1-11D7-8645000102C1865D.
Schultz-Ela, D.D., 2003. Origin of drag folds bordering salt diapirs. AAPG Bull. 87 (5), 757–780. https://doi.org/10.1306/12200201093.
Schultz-Ela, D.D., Jackson, M.P.A., Vendeville, B.C., 1993. Mechanics of active salt diapirism. Tectonophysics 228, 275–312.
Sclater, J.G., Christie, P.A.F., 1980. Continental stretching: an explanation of the Post-Mid-cretaceous subsidence of the central North-Sea Basin. J. Geophys. Res. 85 (B7), 3711–3739. https://doi.org/10.1029/JB085iB07p03711.
Searle, M.P., 2007. Structural geometry, style and timing of deformation in the Hawasina Window, Al Jabal al Akhdar and Saih Hatat culminations, Oman Mountains. GeoArabia 12 (2), 99–130.
Searle, M.P., Cherry, A.G., Ali, M.Y., Cooper, D.J.W., 2014. Tectonics of the Musandam Peninsula and northern Oman Mountains: from ophiolite obduction to continental collision. GeoArabia 19, 135–174.
Snidero, M., Muñoz, J.A., Carrera, N., Butillé, M., Mencos, J., Motamedi, H., Piryaei, A., Sàbat, F., 2019. Temporal evolution of the Darmadan salt diapir, eastern Fars region, Iran. Tectonophysics 766, 115–130. https://doi.org/10.1016/j.tecto.2019.06.006.
Snidero, M., Carrera, N., Mencos, J., Butillé, M., Granado, P., Tavani, S., Lopez-Mir, B., Sabat, F., Muñoz, J.A., 2020. Diapir kinematics in a multi-layer salt system from the eastern Persian Gulf. Mar. Pet. Geol. 117 https://doi.org/10.1016/j.marpetgeo.2020.104402.
Stern, R.J., Johnson, P.R., 2010. Continental lithosphere of the Arabian Plate: a geologic, petrologic, and geophysical synthesis. Earth Sci. Rev. 101 (1–2), 29–67. https://doi.org/10.1016/j.earscirev.2010.01.002.
Stewart, S.A., 2016. Structural geology of the Rub' Al-Khali Basin, Saudi Arabia. Tectonics 35, 2417–2438. https://doi.org/10.1002/2016TC004212.
Stewart, S.A., 2017. Hormuz salt distribution and influence on structural style in NE Saudi Arabia. Pet. Geosci. 24, 143–158. https://doi.org/10.1144/petgeo2017-011.
Stewart, S.A., Coward, M.P., 1995. Synthesis of salt tectonics in the southern North Sea, UK. Mar. Pet. Geol. 12 (5), 457–475. https://doi.org/10.1016/0264-8172(95)91502-G.
Stöcklin, J., 1968. Structural history and tectonics of Iran: a review. AAPG Bull. 52 (7), 1229–1258. https://doi.org/10.1306/5D25C4A5-16C1-11D7-8645000102C1865D.
Tavakoli-Shirazi, S., Frizon de Lamotte, D., Wrobel-Daveau, J.-C., Ringenbach, J.-C., 2013. Pre-Permian uplift and diffuse extensional deformation in the High Zagros Belt (Iran): integration in the geodynamic evolution of the Arabian plate. Arab. J. Geosci. 6 (7), 2329–2342. https://doi.org/10.1007/s12517-012-0542-5.
Trusheim, F., 1960. Mechanism of salt migration in northern Germany. AAPG Bull. 44, 1519–1540. https://doi.org/10.1306/0BDA61CA-16BD-11D7-8645000102C1865D.
Vendeville, B.C., 2005. Salt tectonics driven by sediment progradation: Part I—Mechanics and kinematics. AAPG Bull. 89 (8), 1071–1079. https://doi.org/10.1306/03310503063.
Vendeville, B.C., Jackson, M.P.A., 1992. The rise of diapirs during thin-skinned extension. Mar. Pet. Geol. 9 (4), 331–354. https://doi.org/10.1016/0264-8172(92)90047-I.
Vendeville, B.C., Nilsen, K.T., 1995. Episodic growth of salt diapirs driven by horizontal shortening. Salt, sediment, and hydrocarbons: Gulf Coast Section-SEPM Foundation 16th Annual Research Conference, Houston, Texas. Soc. Explor. Paleontol. Mineral. Found. 285–295.
Vergés, J., Emami, H., Garcés, M., Beamud, E., Homke, S., Skott, P., 2018. Zagros foreland fold belt timing across Lurestan to constrain Arabia–Iran collision. In: Farzipour-Saein, A. (Ed.), Tectonic and Structural Framework of the Zagros Fold-Thrust Belt, 3. Elsevier, pp. 29–52. https://doi.org/10.1016/B978-0-12-815048-1.00003-2.
Warren, J.K., 2016. Evaporites: A Geological Compendium. Springer, 2nd ed, p. 1813.
Warsitzka, M., Kley, J., Kukowski, N., 2013. Salt diapirism driven by differential loading — some insights from analogue modelling. Tectonophysics 591, 83–97. https://doi.org/10.1016/j.tecto.2011.11.018.
Warsitzka, M., Kley, J., Kukowski, N., 2015. Analogue experiments of salt flow and pillow growth due to basement faulting and differential loading. Solid Earth 6, 9–31. https://doi.org/10.5194/se-6-9-2015.
Weijermars, R., Jackson, M.P.A., Vendeville, B.C., 1993. Rheological and tectonic modeling of salt provinces. Tectonophysics 217, 143–174. https://doi.org/10.1016/0040-1951(93)90208-2.